

1 **Rapid mass growth and enhanced light extinction of atmospheric aerosols during the heating**  
2 **season haze episodes in Beijing revealed by aerosol-chemistry-radiation-boundary layer**  
3 **interaction**

4

5 Zhuohui Lin<sup>1</sup>, Yonghong Wang<sup>2,3</sup>, Feixue Zheng<sup>1</sup>, Ying Zhou<sup>1</sup>, Yishuo Guo<sup>1</sup>, Zemin Feng<sup>1</sup>, Chang  
6 Li<sup>1</sup>, Yusheng Zhang<sup>1</sup>, Simo Hakala<sup>2</sup>, Tommy Chan<sup>2</sup>, Chao Yan<sup>2</sup>, Kaspar R. Daellenbach<sup>2</sup>, Biwu  
7 Chu<sup>3</sup>, Lubna Dada<sup>2</sup>, Juha Kangasluoma<sup>1,2</sup>, Lei Yao<sup>2</sup>, Xiaolong Fan<sup>1</sup>, Wei Du<sup>2</sup>, Jing Cai<sup>2</sup>, Runlong  
8 Cai<sup>2</sup>, Tom V. Kokkonen<sup>2,4</sup>, Putian Zhou<sup>2</sup>, Lili Wang<sup>5</sup>, Tuukka Petäjä<sup>2,4</sup>, Federico Bianchi<sup>1,2</sup>, Veli-  
9 Matti Kerminen<sup>2,4</sup>, Yongchun Liu<sup>1</sup>, and Markku Kulmala<sup>1,2,4</sup>

10

11 <sup>1</sup>Aerosol and Haze Laboratory, Beijing Advanced Innovation Center for Soft Matter Science and  
12 Engineering, Beijing University of Chemical Technology, Beijing, China

13 <sup>2</sup>Institute for Atmospheric and Earth System Research / Physics, Faculty of Science, University of  
14 Helsinki, Finland

15 <sup>3</sup>Research Center for Eco-Environmental Sciences, Chinese Academy of Science, Beijing, China

16 <sup>4</sup>Joint international research Laboratory of Atmospheric and Earth System sciences (JirLATEST),  
17 Nanjing University, Nanjing, China

18 <sup>5</sup>State Key Laboratory of Atmospheric Boundary Layer Physics and Atmospheric Chemistry  
19 (LAPC), Institute of Atmospheric Physics, Chinese Academy of Sciences, Beijing 100029, China

20

21

22

23 Corresponding author: Yonghong Wang

24 E-mail: yonghongwang@rcees.ac.cn

25 Revised to: Atmospheric Chemistry and Physics

26

## 27   **Abstract**

28

29   Despite the numerous studies investigating haze formation mechanism in China, it is still puzzling  
30   that intensive haze episodes could form within hours directly following relatively clean periods.

31   Haze has been suggested to be initiated by the variation of meteorological parameters and then to be  
32   substantially enhanced by aerosol-radiation-boundary layer feedback. However, knowledge on the  
33   detailed chemical processes and the driving factors for extensive aerosol mass accumulation during  
34   the feedback is still scarce. Here, the dependency of the aerosol number size distribution, mass  
35   concentration and chemical composition on the daytime mixing layer height (MLH) in urban  
36   Beijing is investigated. The size distribution and chemical composition-resolved dry aerosol light  
37   extinction is also explored. The results indicate that the aerosol mass concentration and fraction of  
38   nitrate increased dramatically when the MLH decreased from high to low conditions, corresponding  
39   to relatively clean and polluted conditions, respectively. Particles having their dry diameters in the  
40   size of ~400-700 nm, and especially particle-phase ammonium nitrate and liquid water, contributed  
41   greatly to visibility degradation during the winter haze periods. The dependency of aerosol  
42   composition on the MLH revealed that ammonium nitrate and aerosol water content increased the  
43   most during low MLH conditions, which may have further triggered enhanced formation of  
44   sulphate and organic aerosol via heterogeneous reactions. As a result, more sulphate, nitrate and  
45   water soluble organics were formed, leading to an enhanced water uptake ability and increased light  
46   extinction by the aerosols. The results of this study contribute towards a more detailed  
47   understanding of the aerosol-chemistry-radiation-boundary layer feedback that is likely to be  
48   responsible for explosive aerosol mass growth events in urban Beijing.

49

50

51

52

53

54

## 55    **1. Introduction**

56    Despite the recent reduction of air pollutants and their precursors in China between 2013 and 2017,  
57    the current emission and air pollution levels are still substantially high (Wang et al., 2020b; Zheng  
58    et al., 2018). Such high emissions, combined with specific meteorological conditions, frequently  
59    lead to severe haze episodes (An et al., 2019; Wang et al., 2019). Particulate matter, a major air  
60    pollutant, has considerable effects on climate, human health and visibility degradation (Che et al.,  
61    2007; Lelieveld et al., 2015; Spracklen et al., 2008; Wang et al., 2015).

62  
63    During winter haze episodes, a rapid growth of the aerosol mass concentration has commonly been  
64    observed, and this phenomenon seems to be directly affected by meteorological factors (Li et al.,  
65    2018b; Liu et al., 2018, 2019b; Wang et al., 2018a, 2014a). The meteorological conditions and  
66    increased aerosol concentrations are proposed to be interlinked by a feedback loop, called the  
67    aerosol-chemistry-boundary layer feedback, in which aerosol particles reduce both solar radiation  
68    reaching the surface and turbulent kinetic energy (TKE) of the near-surface air (Ding et al., 2016;  
69    Petäjä et al., 2016; Wang et al., 2020d). The reduced TKE owing to aerosol reduce the entrainment  
70    of relatively dry air into the mixing layer from above, which makes the air more humid within the  
71    mixing layer. The increased relative humidity due to decreased surface temperature enhance the  
72    aerosol water uptake ability and promote secondary aerosol formation via aqueous-phase reactions,  
73    enhancing light scattering and causing further reduction of solar radiation reaching the surface. All  
74    of these factors lead to increased stability of mixing layer height and enhanced air pollution in the  
75    mixed layer, which further suppresses the development of boundary layer. As a consequence,  
76    concentrations of primary aerosol particles, water vapor and relative humidity increase, creating  
77    more favourable conditions for homogeneous and heterogeneous reactions on aerosol surfaces or  
78    inside them (Cheng et al., 2016a; Wang et al., 2016; Wu et al., 2018). Such reactions cause rapid  
79    formation of secondary aerosol matter and enhanced light extinction during severe winter haze  
80    episodes. However, more detailed information on the aerosol and reactive gas chemistry during the  
81    aerosol-chemistry-boundary layer feedback and related rapid aerosol mass growth events is still  
82    needed (Liu et al., 2019). For instance, it is still unclear which chemical reactions and which

compounds in the particulate matter play key roles during such rapid mass growth events.

The particle number size distribution and chemical composition are considered to be the most important variables influencing the light extinction by aerosol particles. In the atmosphere, the highest contribution to aerosol light extinction comes from organic compounds, nitrate and sulphate in particles with diameters of 100-1000 nm. This is due to the dominant mass fractions of the aforementioned compounds in aerosols that correspond to the peak intensity of solar radiation at wavelengths around 550 nm (Jimenez et al., 2009; Swietlicki et al., 2008). In addition, light scattering which contributes the most to the light extinction by atmospheric aerosols, can be substantially enhanced by the presence of liquid water in the aerosol (Chen et al., 2014; Liu et al., 2019a; Pan et al., 2009; Wang et al., 2020). Hence, quantifying the response of light extinction to different chemical compounds would be helpful in evaluating the feedbacks associated with secondary aerosol production.

In this study, we focus on the physical and chemical properties of aerosols in Beijing during the winter heating season from October 2018 to February 2019 using state-of-the-art instrumentation. The variation of aerosol chemical composition and the associated light extinction coefficient as a function of the varying mixing layer height are discussed. Our aim is to identify the key chemical components which contribute to the aerosol-chemistry-radiation-boundary layer feedback loop in Beijing.

## **2. Methodology**

### **2.1. Measurement location and instrumentations**

Measurements were conducted between 1 October 2018 and 28 February 2019 at the roof top of the university building at the west campus of Beijing University of Chemical Technology (39.95°N, 116.31°E). This station is located about 150 m away from the nearest road (Zizhuyuan road) and

109 500 m away from the West Third Ring Road, and it is surrounded by commercial properties and  
110 residential dwellings representative of an urban environment. More details on the location can be  
111 found in (Liu et al., 2020; Zhou et al., 2020).  
112  
113 The meteorological data for this work include basic meteorological variables (relative humidity  
114 (RH), temperature, wind speed, wind direction, and visibility) and mixing layer height (MLH)  
115 measured using a weather station (Vaisala Inc., Finland) and a Ceilometer CL51 (Vaisala Inc.,  
116 Finland), respectively. The MLH is defined as the height above the surface, through which  
117 relatively vigorous vertical mixing occurs (Holzworth, 1972), and its value is highly related to the  
118 vertical temperature structure and, so some extent, to a mechanically-induced turbulence (Baxter,  
119 1991). Here, we followed the method introduced earlier by Mönkel et al. (2007) and Eresmaa et al.  
120 (2012) in determining the MLH.  
121  
122 The number size distributions of aerosol particles from 6 nm to 840 nm were measured by a  
123 Differential Mobility Particle Sizer (DMPS) (Aalto et al., 2001). The mass concentration of fine  
124 particulate matter (PM<sub>2.5</sub>) was measured using a Tapered Element Oscillating Microbalance  
125 Dichotomous Ambient Particulate Monitor (TEOM 1405-DF, Thermo Fisher Scientific Inc, USA)  
126 with a total flow rate of 16.67 L/min (Wang et al., 2014).  
127  
128 A time-of-flight aerosol chemical speciation monitor (ToF-ACSM, Aerodyne Research Inc.) was  
129 used to measure the concentrations of non-refractory (NR) components, including sulfate, nitrate,  
130 ammonium, chloride and organics of PM<sub>2.5</sub> (Fröhlich et al., 2013). A PM<sub>2.5</sub> cyclone was deployed on  
131 the rooftop with a flow rate of 3 L /min. The correlation coefficient of PM<sub>2.5</sub> measured by TEOM  
132 and ToF-ACSM is around 0.9, which indicates the consistence of the two datasets. Aerosol was  
133 dried though a Nafion dryer (MD-700-24F-3, PERMA PURE) before entering the ToF- ACSM. The  
134 inlet flow was set at 1.4 cm<sup>3</sup>/s. The particle beam passed through the chamber and reached the  
135 heated porous tungsten surface (T≈600°C). There, the non-refractory PM<sub>2.5</sub> constituents were  
136 vaporized and then ionized by electrons (E<sub>kin</sub>=70eV, emitted by a tungsten filament). The ions were

137 measured by a detector and the data was analyzed using Tofware ver. 2.5.13 within IgorPro ver.  
138 6.3.7.2 (WaveMetrics). The relative ionization efficiencies (RIE) for sulfate, nitrate, ammonium,  
139 chloride and organics applied were 0.86, 1.05, 4.0, 1.5 and 1.4, respectively. Besides RIE  
140 correction, the data also did CO<sub>2</sub>+/- NO<sub>3</sub> artifact correction (Pieber et al., 2016) and collection  
141 efficiency (CE) correction (Middlebrook et al., 2012). The detailed information has been introduced  
142 in Cai et al. (2020). Mass concentrations of ammonium nitrate, ammonium sulfate and ammonium  
143 chloride were determined according to the method introduced by Gysel et al. (2007). The aerosol  
144 liquid water content (AWC) was calculated by the thermodynamic equilibrium model ISORROPIA  
145 II using ToF-ACSM data (Fountoukis and Nenes, 2007).  
146 Highly-oxygenated organic molecules (HOMs) were measured by a chemical ionization long time-  
147 of-flight mass spectrometer equipped with a nitrate chemical ionization source (LToF-CIMS,  
148 Aerodyne Research, Inc. USA) (Jokinen et al., 2012) similar to gas-phase sulfuric acid. The  
149 ambient air was drawn into the ionization source through a stainless-steel tube with a length of ~1.6  
150 m and a diameter of 3/4 inch at a flowrate of ~ 8 L/min. A 30-40 L/min purified air flow and a 4-8  
151 mL/min ultrahigh purity nitrogen flow containing nitric acid were mixed together as the sheath  
152 flow, which is guided through a PhotoIonizer (Model L9491, Hamamatsu, Japan) to produce nitrate  
153 reagent ions. This sheath flow is then introduced into a co-axial laminar flow reactor concentric to  
154 the sample flow. Nitrate ions are pushed to the sample flow layer by an electric field and  
155 subsequently charge analytical molecules. Organic carbon (OC) and element carbon (EC)  
156 concentrations were measured semi-continuously with a 1-hour time resolution using an OC/EC  
157 Analyzer (Model-4, Sunset Lab. Inc.) and time series of ACSM Org and Sunset OC as shown in Fig  
158 S6.  
159 The ammonia is measured by Trace Ammonia analyzer ( Los Gatos Research, Inc.) at atmospheric  
160 ambient levels with high precision (0.2 ppb in 1s) and ultra-fast response (5 Hz).  
161  
162 The air mass history was studied by calculating particle retroplumes using a Lagrangian particle  
163 dispersion model FLEXPART (FLEXible PARTicle dispersion model) ver. 9.02 (Stohl et al., 2005).  
164 The ECMWF (European Centre for Medium-Range Weather Forecast) operational forecast (with

165 0.15° horizontal and 1 h temporal resolution) was used as the meteorological input into the model.  
166 During the measurement period, a new release of 50 000 test particles, distributed evenly between 0  
167 and 100 m above the measurement site, occurred every 1 hour. The released particles were traced  
168 backwards in time for 72 h, unless they exceeded the model boundary (20–60°N, 95–135°E).

170 **2.2. Aerosol light extinction calculation**

171 The aerosol light extinction coefficient was calculated with the Mie-Model, which uses particle  
172 number size distribution, mass concentrations of different aerosol compounds and their refractive  
173 index as inputs (Seinfeld and Pandis, 2006). We introduced a series of assumptions into the Mie-  
174 Model, including 1) “internal mixture” which considers each chemical component in a particle as  
175 homogeneously mixed with each other; 2) all particles are spherical; and 3) particles of different  
176 sizes have the same chemical composition.

177  
178 The practical method introduced under those assumptions in previous studies were found to be  
179 capable of estimating a variation trend of optical property of PM<sub>0.5–20</sub> with a relatively good  
180 accuracy (Lin et al., 2013).

181  
182 Table 1. Summary of the parameters for calculating the average optical refractive index.

183

Species	$\rho_i(\text{g cm}^{-3})$	$n_i$	$k_i$
(NH <sub>4</sub> ) <sub>2</sub> SO <sub>4</sub>	1.760	1.530	0.000
NH <sub>4</sub> NO <sub>3</sub>	1.725	1.554	0.000
NH <sub>4</sub> Cl	1.527	1.639	0.000
Organics	1.400	1.550	0.001
EC	1.500	1.800	0.540

184  
185 The average optical refractive index (AORI) of an internally-mixed particle can be calculated from

186 the optical refractive indices (ORI) of each chemical component by following a mixing rule of  
 187 volume-averaged chemical components as  $AORI = n_{\text{eff}} + k_{\text{eff}} \times i$ , where the real part ( $n_{\text{eff}}$ ) and  
 188 imaginary part ( $k_{\text{eff}}$ ) are given by:

$$n_{eff} = \left( \sum_i n_i \cdot m_i / \rho_i \right) / \left( \sum_i m_i / \rho_i \right) \quad (1)$$

$$k_{eff} = \left( \sum_i k_i \cdot m_i / \rho_i \right) / \left( \sum_i m_i / \rho_i \right) \quad (2)$$

189 Here  $m_i$  and  $\rho_i$  are the mass concentration and density of the component  $i$  in particles,  
 190 respectively, and  $n_i$  and  $k_i$  are the real and imaginary parts of ORI of this component,  
 191 respectively. The parameters for calculating the AORI are summarised in Table 1. The values of  $n_i$   
 192 and  $k_i$  in Table 1 are referenced to the light wavelength of 550 nm.

193  
 194  $Q_{sp,j}$  represents light scattering efficiency of a single particle with diameter  $D_j$ , while  $Q_{ep,j}$   
 195 represents light absorption efficiency. Theoretically,  $Q_{sp,j}$  and  $Q_{ep,j}$  are both the function of  $D_j$   
 196 and the  $AORI_j$  (the AORI of the particle with diameter  $D_j$ ) at a given light wavelength  $\lambda$ , for  
 197 which the complicated calculations were referenced to a previous publication (Lin et al., 2013).  
 198 Regarding the limitations of measurement techniques, the  $AORI_j$  was assumed to be equal to the  
 199  $AORI_{PM2.5}$ , which was determined based on chemical composition of  $PM_{2.5}$ . It is possible to derive  
 200 expressions for the cross sections of a spherical particle exactly. The formulas for  $Q_{sp,j}$  and  $Q_{ep,j}$   
 201 are:

$$Q_{sp,j}(D_j, \lambda, AORI_j) = \frac{2}{\alpha^2} \sum_{k=1}^{\infty} (2k+1) \cdot [|a_k|^2 + |b_k|^2] \quad (3)$$

$$Q_{ep,j}(D_j, \lambda, AORI_j) = \frac{2}{\alpha^2} \sum_{k=1}^{\infty} (2k+1) \cdot \text{Re}[a_k + b_k] \quad (4)$$

203  
 204 where  
 205



$$a_k = \frac{\alpha \psi'_k(y) \psi_k(\alpha) - y \psi'_k(\alpha) \psi_k(y)}{\alpha \psi'_k(y) \xi_k(\alpha) - y \xi'_k(\alpha) \psi_k(y)}$$

$$b_k = \frac{y \psi'_k(y) \psi_k(\alpha) - \alpha \psi'_k(\alpha) \psi_k(y)}{y \psi'_k(y) \xi_k(\alpha) - \alpha \xi'_k(\alpha) \psi_k(y)}$$

with  $y = \alpha m$ .

$$m = n_{eff} + i \cdot k_{eff}$$

$$\alpha = \frac{\pi D_j}{\lambda}$$

with  $\lambda = 550$  nm.

where complex number  $m$  stands for  $AORI_j$ , while  $\alpha$  is the size of the particle, usually expressed as a dimensionless size parameter. The functions  $\psi_k(z)$  and  $\xi_k(z)$  are the Riccati–Bessel functions:

$$\psi_k(z) = \left(\frac{\pi z}{2}\right)^{1/2} J_{k+1/2}(z) \quad (5)$$

$$\xi_k(z) = \left(\frac{\pi z}{2}\right)^{1/2} [J_{k+1/2}(z) + i(-1)^k J_{-k-1/2}(z)] \quad (6)$$

where  $J_{k+1/2}$  and  $J_{-k-1/2}$  are the Bessel functions of the first kind and their footnotes indicate the order of Bessel functions. The Mie theory can serve as the basis of a computational procedure to calculate the scattering and absorption of light by any sphere as a function of wavelength.

According to the Mie-Model,  $b_{sp}$  (light scattering coefficient) and  $b_{ep}$  (light extinction coefficient) can be quantified with Eqs. (5) and (6), respectively.  $b_{ap}$  (light absorption coefficient) is the difference between  $b_{ep}$  and  $b_{sp}$ , which equals zero, when  $k_i$  equals zero or very small. Optical properties including  $b_{ep}$ ,  $b_{sp}$  and  $b_{ap}$  to be discussed later are all referenced to light wavelength of 550 nm.

$$b_{sp} = \sum_j b_{sp,j} = \sum_j \frac{\pi D_j^2}{4} \cdot Q_{sp,j}(D_j, \lambda, AORI_j) \cdot N_j \quad (7)$$

$$b_{ep} = \sum_j b_{ep,j} = \sum_j \frac{\pi D_j^2}{4} \cdot Q_{ep,j}(D_j, \lambda, AORI_j) \cdot N_j \quad (8)$$

231

232

233 In Eqs. (7) and (8),  $D_j$  stands for the median Stokes diameter in the  $j$ -th particle size range and  $N_j$

234 is the number concentration of particles with diameter,  $D_j$ .

235

### 236 3. Results and discussion

#### 3.1. An over of the measurement campaign

The time series particle number size distribution from 6 nm to 840 nm, mass concentrations of nitrate, organics, sulfate, ammonium and chloride in NR\_PM<sub>2.5</sub> (non-refractory PM<sub>2.5</sub>) and PM<sub>2.5</sub>, concentration of HOMs and OC are shown in Figure 1(a), (b) and (c). The statistics of these compounds are summarized in Table S1. In general, they showed similar variation patterns (Figure S2 and S3). These concentrations showed high values during haze event than clean days and increased significantly during night time. As shown in Figure 1(b), the rapid mass growth during the heating season in Beijing is related to the rapid growth in nitrate concentration. At the same time, the haze events (PM<sub>2.5</sub> concentration  $\geq 75 \mu\text{g}/\text{m}^3$  and lasting more than one day) are accompanied by particle size growth (Figure 1(a)). To further study which particle size possesses the highest light extinction efficiency during the haze events, and to what extent nitrates contribute to light extinction with the variation of MLH, a case of rapid rapid aerosol mass growth event is selected for further study.

### 3.2. Typical case of rapid aerosol mass growth episodes affected by aerosol-chemistry-boundary layer interactions

An example of rapid aerosol mass growth in urban wintertime Beijing is illustrated in Figure 2, where the haze accumulation was associated with a rapid PM<sub>2.5</sub> mass concentration increase from 8.5 µg/m<sup>3</sup> to more than 100 µg/m<sup>3</sup> in less than 7 hours. A haze episode started on afternoon 20 February 2019 under stagnant meteorological conditions with low wind speeds and elevated ambient relative humidity (Figure S4). The polluted periods during this case occurred under southerly wind transport conditions, whereas clean air masses originated from the north-westerly regions (as shown in Figure S5, S6). These are typical features for a haze evolution process in Beijing (Wang et al., 2020b). During the haze periods marked by the shaded areas in Figure 2, an obvious increase of chemical mass concentration was observed by the ToF-ACSM, characterised by high concentrations of secondary aerosol components (nitrate, organics and sulphate) and typically a shallow boundary layer. The mass concentrations of organics, sulphate and nitrate increased dramatically with a decreasing MLH, accounting for 88.5% of NR-PM<sub>2.5</sub> during the rapid aerosol mass growth period. The aerosol mass growth was the fastest for nitrate. The mass concentrations of organic and elemental carbon followed that of NR-PM<sub>2.5</sub>.

The MLH reached its maximum at around 14:00 in the afternoon of 20 February, after which the development of the mixing layer was suppressed and MLH decreased with the arrival of pollution (Figure 2a). Previous studies have shown that the aerosol-radiation-boundary layer feedback contributes to a rapid enhancement of air pollution (Petäjä et al., 2016; Wang et al., 2020d). High concentrations of aerosol particles obscure downward radiation, as a result of which the surface temperature and sensitive heat flux decrease and the development of mixing layer height is suppressed. Recent studies have gradually realized that the facilitation of various chemical processes play a non-negligible role in the aerosol-radiation-boundary layer feedback (Liu.Q et al., 2018; Liu. Z et al., 2019). Therefore, it is important to identify and quantify the role of different specific chemical species and particle size ranges in reducing atmospheric radiation and extinction.

Figure 3 shows the contributions of size and chemical composition-resolved dry aerosol to light extinction during the investigated period. As the pollution intensified and MLH decreased (Fig 2c), the light extinction of atmospheric aerosols increased significantly. Assuming that particles of different sizes have the same chemical composition as PM<sub>2.5</sub> (organics, NH<sub>4</sub>NO<sub>3</sub>, EC, (NH<sub>4</sub>)<sub>2</sub>SO<sub>4</sub>, NH<sub>4</sub>Cl), the light extinction of particles in the size range of 300-700 nm increased significantly from the relative clean period to the polluted period (namely from 12:00 to 16:00). During relatively clean conditions, the contributions of organics, NH<sub>4</sub>NO<sub>3</sub>, EC, (NH<sub>4</sub>)<sub>2</sub>SO<sub>4</sub> and NH<sub>4</sub>Cl to the total aerosol light extinction were 42%, 23%, 18%, 11% and 7%, respectively. The contribution of NH<sub>4</sub>NO<sub>3</sub> to aerosol light extinction reached 40% during the heavily polluted period. Based on the observation it is likely that the increased light extinction by aerosols reduced solar radiation reaching the surface, so that the development of the boundary layer was suppressed.

### **3.3. Connection between the aerosol chemical composition, light extinction, size distribution and MLH during the heating season**

To better characterize the effect of the chemical composition of dry aerosols and the PNSD (particle number size distribution) light extinction under different MLH conditions, the daytime (8:00 – 16:00 LT) measurement data from October 2018 to February 2019 were selected for further analysis. As shown by Figure 4 and consistent with other observations in Beijing (Tang et al., 2016; Wang et al., 2020c), there was a general tendency for the PM<sub>2.5</sub> mass concentration to increase with a decreasing MLH. Organic compounds and nitrate were the most abundant fractions of the daytime aerosol mass composition, contributing together approximately 70% to total NR-PM<sub>2.5</sub> mass concentration. With a decreasing MLH, the fraction of nitrate mass in NR-PM<sub>2.5</sub> slightly increased while that of organics decreased. This feature makes the aerosol more hygroscopic under low MLH conditions typical for heavily polluted periods. The increased nitrate fraction in the aerosol could also enhance the formation of other secondary aerosol components (Xue et al., 2019). Note that some fraction of aerosol nitrate could consist of organic nitrate originating from reaction of peroxy

292 radical with nitric oxide; however, it is difficult to distinguish organic nitrate from inorganic nitrate  
293 at the moment due to instrumental limitations (Fröhlich et al., 2013).

294  
295 Figure 5 depicts the calculated daytime light extinction of the dry aerosol as a function of the MLH,  
296 separated by different size ranges and chemical components. We may see that in general, particles  
297 with dry diameters in the range of 300-700 nm explains more than 80% of the total aerosol light  
298 extinction (Figure 5b). Similar to their share in NR-PM<sub>2.5</sub>, the fraction of light extinction by  
299 ammonium nitrate increased and that of organics decreased during the lowest MLH conditions  
300 corresponding to the heavy pollution periods (Figure 5d). There are also apparent differences in the  
301 relative contribution of different particle size ranges to light extinction in different MLH conditions:  
302 with a decreasing MLH, the contribution of particles with dry dimeters larger than about 400-  
303 500 nm clearly increased while that of sub-300 nm particles notably decreased. This indicates that  
304 the enhanced light extinction by the dry aerosol at low MLH conditions was not only due the more  
305 abundant aerosol mass concentration, but also due to the growth of individual particles to optically  
306 more active sizes.

307  
308 At relative humidity larger than about 70%, aerosol liquid water gives a significant contribution to  
309 the aerosol mass concentration and often a dominant contribution to the aerosol light extinction  
310 (Titos et al., 2016). This has important implications for the aerosol-chemistry-radiation-boundary  
311 layer feedback, when considering our findings listed above and further noting that heavy pollution  
312 periods are often accompanied by high values of RH in Beijing (Zhong et al., 2018). First,  
313 compared to clean or moderately-polluted conditions, the enhancement in the aerosol light  
314 extinction under polluted is probably much larger than that illustrated in Figure 5. Second, the high  
315 aerosol water content under polluted conditions promotes many kinds of chemical reactions taking  
316 place on the surface or inside aerosol particles.

317

### 3.4. Aerosol-chemistry-radiation-boundary layer interaction

In order to further investigate the interaction between MLH and chemical compounds (either observed or calculated), we divided the observed PM<sub>2.5</sub> concentrations into highly polluted and less polluted conditions using a threshold value of 75 µg /m<sup>3</sup> for PM<sub>2.5</sub>. The organics, nitrate, ammonium, sulfate, chloride, HOM, aerosol water content (AWC) and PM<sub>2.5</sub> as a function of the mixing layer height during both highly polluted and less polluted conditions are shown in Figure 6. The fitted relationships connecting the concentrations of different chemical compounds to the reduction of MLH under highly and less polluted conditions allowed us to estimate the net mass concentration increase of each compound due to secondary formation and aerosol-chemical-boundary layer feedback under highly polluted conditions (shaded areas in Figure 6). It is worth noting that AWC, nitrate and sulfate increased the most as the MLH decreased, as represented by the large shaded areas in Figs. 6 (h), (b) and (c). The increases of these components are significant as tested (Supplement Information). The day-time nitrate in aerosol is formed predominately via the reaction of nitric acid and ammonium, while nitric acid is produced from gas phase reaction of nitrogen dioxide and hydroxy radical (Seinfeld and Pandis, 2006). High concentrations of daytime nitrate aerosols indicate efficient production of gas phase nitric acid, its partitioning into liquid aerosol and its fast neutralization by abundant ammonia (Li et al., 2018a; Pan et al., 2016; Wang et al., 2020). A recent study shows that condensation of nitric acid and ammonia could promote fast growth of newly formed particle in urban environment condition (Wang et al., 2020d). Another possibility is that ammonium nitrate is formed rapidly on particle surfaces due to the hydrolysis of dinitrogen pentoxide (N<sub>2</sub>O<sub>5</sub>) during daytime, as the AWC increased significantly (Wang et al., 2014; Wang et al., 2020). However, a quantitative distinction between the two formation pathways for nitrate formation is not possible in this study. The dramatic increase of nitrate aerosol could also promote the formation of sulfate by heterogeneous reactions (Cheng et al., 2016b; Wang et al., 2016). The concentration of HOMs showed a slight increase as the MLH decreased, which suggests that also the formation of HOMs is enhanced with an increased level of air pollution. This phenomenon should be further investigated as HOMs can substantially contribute to the secondary

346 organic aerosol formation.

347

348 Figure 7 displays the dry aerosol light extinction by different chemical compounds in the same way  
349 as Figure 6 did for aerosol mass concentrations. The aerosol light extinction is directly related to the  
350 reduction of solar radiation reaching the surface, assuming that aerosol chemical components are  
351 vertically nearly homogeneously distributed. The light extinction from ammonium nitrate,  
352 ammonium sulfate and organics showed significantly increased contributions under highly polluted  
353 conditions (low MLH) as compared with less polluted conditions. To the contrary, no such  
354 enhancement was observed for ammonium chloride or element carbon (Figs. 7 (d) and (e)). In case  
355 of EC this is an expected result, as it originates solely from primary sources. The formation of  
356 particle phase chloride have secondary sources from chlorine atom-initiated oxidation of volatile  
357 organic compounds, so that the resulting oxidation products could contribute to the observed  
358 chloride (Wang and Ruiz, 2017; Wang et al., 2019a).

359

360 To better illustrate the combined effects of secondary aerosol formation and associated feedback on  
361 the daytime mass concentrations and light extinction due to different chemical components, we  
362 scaled these quantities by either the total PM<sub>2.5</sub> mass concentration or EC concentration and plotted  
363 them as a function of MLH (Fig. 8). With the average level of PM<sub>2.5</sub> measured by TEOM and ToF-  
364 ACSM, the latter scaling minimizes the boundary layer accumulation effect on our analysis, as EC  
365 originates from primary emission sources (Cao et al., 2006). As shown in Fig. 8a, organics with  
366 their mass fraction of 61% were the most abundant component in PM<sub>2.5</sub> under high MLH  
367 conditions, followed by nitrate and ammonium with their mass fractions of 22% and 13%,  
368 respectively. The aerosol was estimated to be rather dry under high MLH conditions ( $AWC/PM_{2.5} =$   
369 0.03). However, with the decreasing MLH, the fraction of nitrate and the AWC to PM<sub>2.5</sub> ratio  
370 increased up to 45% and 0.2, respectively. This clearly indicates rapid nitrate formation and  
371 dramatic increase of the aerosol water uptake from less polluted conditions to intensive haze  
372 pollution. Compared with EC (Fig.8c), the concentrations of organic compounds, nitrate, sulfate  
373 and ammonium increased by factors of 1.5, 6.3, 4.8 and 4.9 respectively, from the highest to the

lowest MLH conditions. Thus, although organics remained as the second most abundant aerosol component after nitrate under haze conditions, secondary formation and associated feedback from less to highly polluted conditions were clearly stronger for both sulfate and ammonium. Efficient sulfate production associated with haze formation has been reported in several studies conducted in China (Cheng et al., 2016; Xie et al., 2015; Xue et al., 2016). Ammonium production during haze formation is tied with neutralization of acidic aerosol by ammonia, which was apparently present abundantly in the gas phase. Compared with the EC concentration, light extinction by (NH<sub>4</sub>NO<sub>3</sub>) increased the most from the highest MLH conditions (248 M m<sup>-1</sup>/μg m<sup>-3</sup>) to the lowest MLH conditions (1150 M m<sup>-1</sup>/μg m<sup>-3</sup>) as shown by Figure 8b. Overall, the rapid growth of nitrate aerosol mass, together with abundant concentration of organic aerosol, were the main cause of the light extinction for dry aerosol under haze formation.

The mechanism governing the aerosol-chemistry-radiation-boundary layer feedback for the rapid growth of atmospheric aerosol is illustrated in Fig. 9. As a result of reduction in solar radiation and atmospheric heating, a variety of chemical reactions in the gas phase and on particle surfaces or inside them are enhanced with an increased relative humidity and AWC. Such conditions are unfavorable for the dispersion of pollutants, which further enhances atmospheric stability. The formation of hydrophilic compounds, e.g., nitrate, sulfate and oxygenated organic compounds, result in enhanced water uptake by aerosol particles, which will essentially increase heterogeneous reactions associated with these particles. As a result, the aerosol mass and size increase, light extinction is enhanced, and the development of the mixing layer is depressed. At the same time, aerosol precursors concentrated within a shallower mixing layer lead to enhanced production rate of aerosol components in both gas and aerosol phases, especially nitrate but also other secondary aerosol. The increased concentrations of aerosol will further enhance this positive loop.

#### 4. Conclusions



401 We investigated the synergetic variations of aerosol chemical composition and mixing layer height  
402 during the daytime in urban Beijing. Significant dependency of the sharp increase of ammonium  
403 nitrate and aerosol water content with the occurrence of the explosive aerosol mass growth events  
404 were observed. We showed that these two components drove a positive aerosol-chemistry-radiation-  
405 boundary layer feedback loop, which played an important role in the explosive aerosol mass growth  
406 events. A plausible explanation is that the increased aerosol water content at low mixing layer  
407 heights provides favorable conditions for heterogeneous reactions for nitrate and sulfate production  
408 and neutralization by ammonia. The significant formation of secondary aerosol increases the  
409 concentration of aerosol particles in the diameter range 300-700 nm, which effectively reduces the  
410 solar radiation reaching the surface and further enhances the aerosol-chemistry-radiation-boundary  
411 layer feedback loop. Our analysis connects the aerosol light extinction to a reduction in the mixing  
412 layer height, which suppresses the volume into which air pollutants are emitted and leads to an  
413 explosive aerosol mass growth. Our results indicate that reduction of ammonium and nitrate  
414 concentration in aerosol could weaken the aerosol-radiation-chemistry-boundary layer feedback  
415 loop, which could thereby reduce heavy haze episodes in Beijing.

## 416 **5. Acknowledgements**

417 This work was supported by the funding from Beijing University of Chemical Technology. The  
418 European Research Council via advanced grant ATM-GTP (project no. 742206) and Academy of  
419 Finland via Academy professor project of M. K.

## 420 **6. Competing financial interests**

421 The authors declare no competing financial interests.

## **7. Author contributions**

422 YW and MK initiated the study. ZL, YW, FZ, YZ, YG, ZF, CL, YZ, TC, CY, KD, BC, JK, LY, XF,  
423 WD, JC and YL conducted the longtime measurements. ZL, YW, LD, RC, SH, PZ, LW, VK, YL

424 and MK interpreted the data. ZL, YW and VK wrote the manuscript.

425

426

427

428

- Aalto, P., Hämeri, K., Becker, E. D. O., Weber, R., Salm, J., Mäkelä, J. M., Hoell, C., O'Dowd, C. D., Karlsson, H., Hansson, H., Väkevä M., Koponen, I. K., Buzorius, G. and Kulmala, M.: Physical characterization of aerosol particles during nucleation events, *Tellus, Series B: Chemical and Physical Meteorology*, 53(4), 344–358, doi:10.3402/tellusb.v53i4.17127, 2001.
- An, Z., Huang, R.-J., Zhang, R., Tie, X., Li, G., Cao, J., Zhou, W., Shi, Z., Han, Y., Gu, Z. and Ji, Y.: Severe haze in northern China: A synergy of anthropogenic emissions and atmospheric processes, *Proceedings of the National Academy of Sciences*, 116(18), 8657 LP – 8666, doi:10.1073/pnas.1900125116, 2019.
- Baxter, R.: Determination of mixing heights from data collected during the 1985 SCCCAMP field program, *Journal of Applied Meteorology*, 30(5), 598–606, doi:10.1175/1520-0450(1991)030<0598:DOMHFD>2.0.CO;2, 1991.
- Cai, J., Chu, B., Yao, L., Yan, C., Heikkinen, L. M., Zheng, F., Li, C., Fan, X., Zhang, S., Yang, D., Wang, Y., Kokkonen, T. V., Chan, T., Zhou, Y., Dada, L., Liu, Y., He, H., Paasonen, P., Kujansuu, J. T., Petäjä, T., Mohr, C., Kangasluoma, J., Bianchi, F., Sun, Y., Croteau, P. L., Worsnop, D. R., Kerminen, V.-M., Du, W., Kulmala, M., and Daellenbach, K. R.: Size-segregated particle number and mass concentrations from different emission sources in urban Beijing, *Atmospheric Chemistry and Physics*, 20, 12721-12740, 10.5194/acp-20-12721-2020, 2020.
- Cao, G., Zhang, X. and Zheng, F.: Inventory of black carbon and organic carbon emissions from China, *Atmospheric Environment*, 40(34), 6516–6527, doi:10.1016/j.atmosenv.2006.05.070, 2006.
- Che, H., Zhang, X., Li, Y., Zhou, Z. and Qu, J. J.: Horizontal visibility trends in China 1981-2005, *Geophysical Research Letters*, 34(24), doi:10.1029/2007GL031450, 2007.
- Chen, J., Zhao, C. S., Ma, N. and Yan, P.: Aerosol hygroscopicity parameter derived from the light scattering enhancement factor measurements in the North China Plain, *Atmos. Chem. Phys*, 14, 8105–8118, doi:10.5194/acp-14-8105-2014, 2014.
- Cheng, Y., Zheng, G., Wei, C., Mu, Q., Zheng, B., Wang, Z., Gao, M., Zhang, Q., He, K., Carmichael, G., Pöschl, U. and Su, H.: Reactive nitrogen chemistry in aerosol water as a source of sulfate during haze events in China, *Science Advances*, 2(12), e1601530–e1601530,

doi:10.1126/sciadv.1601530, 2016b.

Ding, A. J., Huang, X., Nie, W., Sun, J. N., Kerminen, V. M., Petäjä T., Su, H., Cheng, Y. F., Yang, X. Q., Wang, M. H., Chi, X. G., Wang, J. P., Virkkula, A., Guo, W. D., Yuan, J., Wang, S. Y., Zhang, R. J., Wu, Y. F., Song, Y., Zhu, T., Zilitinkevich, S., Kulmala, M. and Fu, C. B.: Enhanced haze pollution by black carbon in megacities in China, *Geophysical Research Letters*, 43(6), 2873–2879, doi:10.1002/2016GL067745, 2016.

Eresmaa, N., Härkönen, J., Joffre, S. M., Schultz, D. M., Karppinen, A. and Kukkonen, J.: A Three-Step Method for Estimating the Mixing Height Using Ceilometer Data from the Helsinki Testbed, *Journal of Applied Meteorology and Climatology*, 51(12), 2172–2187, doi:10.1175/JAMC-D-12-058.1, 2012.

Fountoukis, C. and Nenes, A.: ISORROPIA II: a computationally efficient thermodynamic equilibrium model for

$K^+$ – $Ca^{2+}$ – $Mg^{2+}$ – $NH_4^+$ – $Na^+$ – $SO_4^{2-}$ – $NO_3$ , *Atmospheric Chemistry and Physics*, 7(17), 4639–4659, doi:10.5194/acp-7-4639-2007, 2007.

Fröhlich, R., Cubison, M. J., Slowik, J. G., Bukowiecki, N., Prevôt, A. S. H., Baltensperger, U., Schneider, J., Kimmel, J. R., Gonin, M., Rohner, U., Worsnop, D. R. and Jayne, J. T.: The ToF-ACSM: A portable aerosol chemical speciation monitor with TOFMS detection, *Atmospheric Measurement Techniques*, 6(11), 3225–3241, doi:10.5194/amt-6-3225-2013, 2013.

Gysel, M., Crosier, J., Topping, D. O., Whitehead, J. D., Bower, K. N., Cubison, M. J., Williams, P. I., Flynn, M. J., McFiggans, G. B. and Coe, H.: Closure study between chemical composition and hygroscopic growth of aerosol particles during TORCH2, *Atmospheric Chemistry and Physics*, 7(24), 6131–6144, doi:10.5194/acp-7-6131-2007, 2007.

Holzworth, G. C.: Mixing heights, wind speeds, and potential for urban air pollution throughout the contiguous united states, , 118, 1972.

Jimenez, J. L., Canagaratna, M. R., Donahue, N. M., Prevot, A. S. H., Zhang, Q., Kroll, J. H., DeCarlo, P. F., Allan, J. D., Coe, H., Ng, N. L., Aiken, A. C., Docherty, K. S., Ulbrich, I. M., Grieshop, A. P., Robinson, A. L., Duplissy, J., Smith, J. D., Wilson, K. R., Lanz, V. A., Hueglin, C., Sun, Y. L., Tian, J., Laaksonen, A., Raatikainen, T., Rautiainen, J., Vaattovaara, P., Ehn, M.,

Kulmala, M., Tomlinson, J. M., Collins, D. R., Cubison, M. J., Dunlea, E. J., Huffman, J. A., Onasch, T. B., Alfarra, M. R., Williams, P. I., Bower, K., Kondo, Y., Schneider, J., Drewnick, F., Borrmann, S., Weimer, S., Demerjian, K., Salcedo, D., Cottrell, L., Griffin, R., Takami, A., Miyoshi, T., Hatakeyama, S., Shimono, A., Sun, J. Y., Zhang, Y. M., Dzepina, K., Kimmel, J. R., Sueper, D., Jayne, J. T., Herndon, S. C., Trimborn, A. M., Williams, L. R., Wood, E. C., Middlebrook, A. M., Kolb, C. E., Baltensperger, U. and Worsnop, D. R.: Evolution of organic aerosols in the atmosphere, *Science*, 326(5959), 1525–1529, doi:10.1126/science.1180353, 2009.

Jokinen, T., Sipilä M., Junninen, H., Ehn, M., Lönn, G., Hakala, J., Petäjä T., Mauldin, R. L., Kulmala, M. and Worsnop, D. R.: Atmospheric sulphuric acid and neutral cluster measurements using CI-APi-TOF, *Atmospheric Chemistry and Physics*, 12(9), 4117–4125, doi:10.5194/acp-12-4117-2012, 2012.

Lelieveld, J., Evans, J. S., Fnais, M., Giannadaki, D. and Pozzer, A.: The contribution of outdoor air pollution sources to premature mortality on a global scale, *Nature*, 525(7569), 367–371, doi:10.1038/nature15371, 2015.

Li, H., Zhang, Q., Zheng, B., Chen, C., Wu, N., Guo, H., Zhang, Y., Zheng, Y., Li, X. and He, K.: Nitrate-driven urban haze pollution during summertime over the North China Plain, *Atmospheric Chemistry and Physics*, 18(8), 5293–5306, doi:10.5194/acp-18-5293-2018, 2018a.

Li, J., Sun, J., Zhou, M., Cheng, Z., Li, Q., Cao, X. and Zhang, J.: Observational analyses of dramatic developments of a severe air pollution event in the Beijing area, *Atmospheric Chemistry and Physics*, 18(6), 3919–3935, doi:10.5194/acp-18-3919-2018, 2018b.

Lin, Z. J., Tao, J., Chai, F. H., Fan, S. J., Yue, J. H., Zhu, L. H., Ho, K. F. and Zhang, R. J.: Impact of relative humidity and particles number size distribution on aerosol light extinction in the urban area of Guangzhou, *Atmospheric Chemistry and Physics*, 13(3), 1115–1128, doi:10.5194/acp-13-1115-2013, 2013.

Liu, G., Xin, J., Wang, X., Si, R., Ma, Y., Wen, T., Zhao, L., Zhao, D., Wang, Y. and Gao, W.: Impact of the coal banning zone on visibility in the Beijing-Tianjin-Hebei region, *Science of the Total Environment*, 692, 402–410, doi:10.1016/j.scitotenv.2019.07.006, 2019a.

Liu, Q., Jia, X., Quan, J., Li, J., Li, X., Wu, Y., Chen, D., Wang, Z. and Liu, Y.: New positive

feedback mechanism between boundary layer meteorology and secondary aerosol formation during severe haze events, *Scientific Reports*, 8(1), doi:10.1038/s41598-018-24366-3, 2018.

Liu, Y., Zhang, Y., Lian, C., Yan, C. and Feng, Z.: The promotion effect of nitrous acid on aerosol formation in wintertime Beijing : possible contribution of traffic-related emission, *Atmos. Chem. Phys. Discuss.*, 2020(February), 1–43, doi:10.5194/acp-2020-150, 2020.

Liu, Z., Hu, B., Ji, D., Cheng, M., Gao, W., Shi, S., Xie, Y., Yang, S., Gao, M., Fu, H., Chen, J. and Wang, Y.: Characteristics of fine particle explosive growth events in Beijing, China: Seasonal variation, chemical evolution pattern and formation mechanism, *Science of the Total Environment*, 687, 1073–1086, doi:10.1016/j.scitotenv.2019.06.068, 2019b.

Münkel, C., Eresmaa, N., Räsänen, J. and Karppinen, A.: Retrieval of mixing height and dust concentration with lidar ceilometer, *Boundary-Layer Meteorology*, 124(1), 117–128, doi:10.1007/s10546-006-9103-3, 2007.

Pan, X. L., Yan, P., Tang, J., Ma, J. Z., Wang, Z. F., Gbaguidi, A. and Sun, Y. L.: Observational study of influence of aerosol hygroscopic growth on scattering coefficient over rural area near Beijing mega-city, *Atmospheric Chemistry and Physics*, 9(19), 7519–7530, doi:10.5194/acp-9-7519-2009, 2009.

Pan, Y., Tian, S., Liu, D., Fang, Y., Zhu, X., Zhang, Q., Zheng, B., Michalski, G. and Wang, Y.: Fossil Fuel Combustion-Related Emissions Dominate Atmospheric Ammonia Sources during Severe Haze Episodes: Evidence from  $^{15}\text{N}$ -Stable Isotope in Size-Resolved Aerosol Ammonium, *Environmental Science and Technology*, 50(15), 8049–8056, doi:10.1021/acs.est.6b00634, 2016.

Petäjä T., Järvi, L., Kerminen, V. M., Ding, A. J., Sun, J. N., Nie, W., Kujansuu, J., Virkkula, A., Yang, X., Fu, C. B., Zilitinkevich, S. and Kulmala, M.: Enhanced air pollution via aerosol-boundary layer feedback in China, *Scientific Reports*, 6, doi:10.1038/srep18998, 2016.

Pieber, S. M., El Haddad, I., Slowik, J. G., Canagaratna, M. R., Jayne, J. T., Platt, S. M., Bozzetti, C., Daellenbach, K. R., Fröhlich, R., Vlachou, A., Klein, F., Dommen, J., Miljevic, B., Jimenez, J. L., Worsnop, D. R., Baltensperger, U. and Prevôt, A. S. H.: Inorganic Salt Interference on  $\text{CO}_2$  in Aerodyne AMS and ACSM Organic Aerosol Composition Studies, *Environmental Science and Technology*, 50(19), 10494–10503, doi:10.1021/acs.est.6b01035, 2016.

Spracklen, D. V., Carslaw, K. S., Kulmala, M., Kerminen, V. M., Sihto, S. L., Riipinen, I., Merikanto, J., Mann, G. W., Chipperfield, M. P., Wiedensohler, A., Birmili, W. and Lihavainen, H.: Contribution of particle formation to global cloud condensation nuclei concentrations, *Geophysical Research Letters*, 35(6), doi:10.1029/2007GL033038, 2008.

Stohl, A., Forster, C., Frank, A., Seibert, P. and Wotawa, G.: Technical note: The Lagrangian particle dispersion model FLEXPART version 6.2, *Atmospheric Chemistry and Physics*, 5(9), 2461–2474, doi:10.5194/acp-5-2461-2005, 2005.

Swietlicki, E., Hansson, H.-C., Hämeri, K., Svenningsson, B., Massling, A., Mcfiggans, G., McMurry, P. H., Petäjä T., Tunved, P., Gysel, M., Topping, D., Weingartner, E., Baltensperger, U., Rissler, J., Wiedensohler, A. and Kulmala, M.: Hygroscopic properties of submicrometer atmospheric aerosol particles measured with H-TDMA instruments in various environments—a review, *Tellus B: Chemical and Physical Meteorology*, 60(3), 432–469, doi:10.1111/j.1600-0889.2008.00350.x, 2008.

Tang, G., Zhang, J., Zhu, X., Song, T., Münkler, C., Hu, B., Schäfer, K., Liu, Z., Zhang, J., Wang, L., Xin, J., Suppan, P. and Wang, Y.: Mixing layer height and its implications for air pollution over Beijing, China, *Atmos. Chem. Phys.*, 16, 2459–2475, doi:10.5194/acp-16-2459-2016, 2016.

Titos, G., Cazorla, A., Zieger, P., Andrews, E., Lyamani, H., Granados-Muñoz, M. J., Olmo, F. J. and Alados-Arboledas, L.: Effect of hygroscopic growth on the aerosol light-scattering coefficient: A review of measurements, techniques and error sources, *Atmospheric Environment*, 141, 494–507, doi:10.1016/j.atmosenv.2016.07.021, 2016.

Vanhanen, J., Mikkilä J., Lehtipalo, K., Sipilä M., Manninen, H. E., Siivola, E., Petäjä T. and Kulmala, M.: Particle size magnifier for nano-CN detection, *Aerosol Science and Technology*, 45(4), 533–542, doi:10.1080/02786826.2010.547889, 2011.

Wang, G., Zhang, R., Gomez, M. E., Yang, L., Zamora, M. L., Hu, M., Lin, Y., Peng, J., Guo, S., Meng, J., Li, J., Cheng, C., Hu, T., Ren, Y., Wang, Y., Gao, J., Cao, J., An, Z., Zhou, W., Li, G., Wang, J., Tian, P., Marrero-Ortiz, W., Secrest, J., Du, Z., Zheng, J., Shang, D., Zeng, L., Shao, M., Wang, W., Huang, Y., Wang, Y., Zhu, Y., Li, Y., Hu, J., Pan, B., Cai, L., Cheng, Y., Ji, Y., Zhang, F., Rosenfeld, D., Liss, P. S., Duce, R. A., Kolb, C. E. and Molina, M. J.: Persistent sulfate

formation from London Fog to Chinese haze, *Proceedings of the National Academy of Sciences of the United States of America*, 113(48), 13630–13635, doi:10.1073/pnas.1616540113, 2016.

Wang, H., Peng, Y., Zhang, X., Liu, H., Zhang, M., Che, H. and Cheng, Y.: Contributions to the explosive growth of PM<sub>2.5</sub> mass due to aerosol – radiation feedback and decrease in turbulent diffusion during a red alert heavy haze in Beijing – Tianjin – Hebei, China, , 17717–17733, 2018a.

Wang, J., Wang, S., Jiang, J., Ding, A., Zheng, M., Zhao, B., Wong, D. C., Zhou, W., Zheng, G., Wang, L., Pleim, J. E. and Hao, J.: Impact of aerosol-meteorology interactions on fine particle pollution during China’s severe haze episode in January 2013, *Environmental Research Letters*, 9(9), doi:10.1088/1748-9326/9/9/094002, 2014a.

Wang, M., Kong, W., Marten, R., He, X.-C., Chen, D., Pfeifer, J., Heitto, A., Kontkanen, J., Dada, L., Kürten, A., Yli-Juuti, T., Manninen, H. E., Amanatidis, S., Amorim, A., Baalbaki, R., Baccarini, A., Bell, D. M., Bertozzi, B., Brüning, S., Brilke, S., Murillo, L. C., Chiu, R., Chu, B., De Menezes, L.-P., Duplissy, J., Finkenzeller, H., Carracedo, L. G., Granzin, M., Guida, R., Hansel, A., Hofbauer, V., Krechmer, J., Lehtipalo, K., Lamkaddam, H., Lampimäki, M., Lee, C. P., Makhmutov, V., Marie, G., Mathot, S., Mauldin, R. L., Mentler, B., Müller, T., Onnela, A., Partoll, E., Petäjä, T., Philippov, M., Pospisilova, V., Ranjithkumar, A., Rissanen, M., Rörup, B., Scholz, W., Shen, J., Simon, M., Sipilä, M., Steiner, G., Stolzenburg, D., Tham, Y. J., Tomé, A., Wagner, A. C., Wang, D. S., Wang, Y., Weber, S. K., Winkler, P. M., Wlasits, P. J., Wu, Y., Xiao, M., Ye, Q., Zauner-Wieczorek, M., Zhou, X., Volkamer, R., Riipinen, I., Dommen, J., Curtius, J., Baltensperger, U., Kulmala, M., Worsnop, D. R., Kirkby, J., Seinfeld, J. H., El-Haddad, I., Flagan, R. C. and Donahue, N. M.: Rapid growth of new atmospheric particles by nitric acid and ammonia condensation, *Nature*, 581(7807), 184–189, doi:10.1038/s41586-020-2270-4, 2020d.

Wang, X., Wang, T., Yan, C., Tham, Y. J., Xue, L., Xu, Z. and Zha, Q.: Large daytime signals of N<sub>2</sub>O<sub>5</sub> and NO<sub>3</sub> inferred at 62 amu in a TD-CIMS: Chemical interference or a real atmospheric phenomenon, *Atmospheric Measurement Techniques*, 7(1), 1–12, doi:10.5194/amt-7-1-2014, 2014b.

Wang, Y., Riva, M., Xie, H. and Heikkinen, L.: Formation of highly oxygenated organic molecules from chlorine atom initiated oxidation of alpha-pinene, *Atmospheric Chemistry and Physics*, 2020,



1–31, doi:10.5194/acp-2019-807, 2020.

Wang, Y., Wang, Y., Wang, L., Petäjä T., Zha, Q., Gong, C., Li, S., Pan, Y., Hu, B., Xin, J. and Kulmala, M.: Increased inorganic aerosol fraction contributes to air pollution and haze in China, *Atmos. Chem. Phys.*, 19, 5881–5888, doi:10.5194/acp-19-5881-2019, 2019b.

Wang, Y., Gao, W., Wang, S., Song, T., Gong, Z., Ji, D., Wang, L., Liu, Z., Tang, G., Huo, Y., Tian, S., Li, J., Li, M., Yang, Y., Chu, B., Petäjä T., Kerminen, V.-M., He, H., Hao, J., Kulmala, M., Wang, Y. and Zhang, Y.: Contrasting trends of PM<sub>2.5</sub> and surface ozone concentrations in China from 2013 to 2017, *National Science Review*, doi:10.1093/nsr/nwaa032, 2020b.

Wang, Y., Chen, Y., Wu, Z., Shang, D., Bian, Y., Du, Z. and Schmitt, S. H.: Mutual promotion between aerosol particle liquid water and particulate nitrate enhancement leads to severe nitrate-dominated particulate matter pollution and low visibility, *Atmos. Chem. Phys.*, (September 2020), 2161–2175, 2020c.

Wang, Y., Yu, M., Wang, Y., Tang, G., Song, T., Zhou, P., Liu, Z., Hu, B., Ji, D., Wang, L., Zhu, X., Yan, C., Ehn, M., Gao, W., Pan, Y., Xin, J., Sun, Y., Kerminen, V.-M., Kulmala, M. and Petäjä T.: Rapid formation of intense haze episodes via aerosol–boundary layer feedback in Beijing, *Atmos. Chem. Phys.*, 20(1), 45–53, doi:10.5194/acp-20-45-2020, 2020d.

Wang, Y. H., Hu, B., Ji, D. S., Liu, Z. R., Tang, G. Q., Xin, J. Y., Zhang, H. X., Song, T., Wang, L. L., Gao, W. K., Wang, X. K. and Wang, Y. S.: Ozone weekend effects in the Beijing-Tianjin-Hebei metropolitan area, China, *Atmos. Chem. Phys.*, 14, 2419–2429, doi:10.5194/acp-14-2419-2014, 2014c.

Wang, Y. H., Liu, Z. R., Zhang, J. K., Hu, B., Ji, D. S., Yu, Y. C. and Wang, Y. S.: Aerosol physicochemical properties and implications for visibility during an intense haze episode during winter in Beijing, *Atmospheric Chemistry and Physics*, 15(6), 3205–3215, doi:10.5194/acp-15-3205-2015, 2015.

Wu, Z., Wang, Y., Tan, T., Zhu, Y., Li, M., Shang, D., Wang, H., Lu, K., Guo, S., Zeng, L. and Zhang, Y.: Aerosol Liquid Water Driven by Anthropogenic Inorganic Salts: Implying Its Key Role in Haze Formation over the North China Plain, *Environmental Science and Technology Letters*, 5(3), 160–166, doi:10.1021/acs.estlett.8b00021, 2018.

Xie, Y., Ding, A., Nie, W., Mao, H., Qi, X., Huang, X., Xu, Z., Kerminen, V. M., Petäjä T., Chi, X., Virkkula, A., Boy, M., Xue, L., Guo, J., Sun, J., Yang, X., Kulmala, M. and Fu, C.: Enhanced sulfate formation by nitrogen dioxide: Implications from in-situ observations at the SORPES station, *Journal of Geophysical Research*, 120(24), 12,679-12,694, doi:10.1002/2015JD023607, 2015.

Xue, J., Yuan, Z., Griffith, S. M., Yu, X., Lau, A. K. H. and Yu, J. Z.: Sulfate Formation Enhanced by a Cocktail of High NO<sub>x</sub>, SO<sub>2</sub>, Particulate Matter, and Droplet pH during Haze-Fog Events in Megacities in China: An Observation-Based Modeling Investigation, *Environmental Science and Technology*, 50(14), 7325–7334, doi:10.1021/acs.est.6b00768, 2016.

Xue, J., Yu, X., Yuan, Z., Griffith, S. M., Lau, A. K. H., Seinfeld, J. H. and Yu, J. Z.: Efficient control of atmospheric sulfate production based on three formation regimes, *Nature Geoscience*, 12(12), 1–6, doi:10.1038/s41561-019-0485-5, 2019.

Zheng, B., Tong, D., Li, M., Liu, F., Hong, C., Geng, G., Li, H., Li, X., Peng, L., Qi, J., Yan, L., Zhang, Y., Zhao, H., Zheng, Y., He, K. and Zhang, Q.: Trends in China’s anthropogenic emissions since 2010 as the consequence of clean air actions, *Atmospheric Chemistry and Physics Discussions*, 1–27, doi:10.5194/acp-2018-374, 2018.

Zhong, J., Zhang, X., Dong, Y., Wang, Y., Liu, C., Wang, J., Zhang, Y. and Che, H.: Feedback effects of boundary-layer meteorological factors on cumulative explosive growth of PM<sub>2.5</sub> during winter heavy pollution episodes in Beijing from 2013 to 2016, *Atmospheric Chemistry and Physics*, 18(1), 247–258, doi:10.5194/acp-18-247-2018, 2018.

Zhou, Y., Dada, L., Liu, Y., Fu, Y., Kangasluoma, J., Chan, T., Yan, C., Chu, B., Daellenbach, K. R., Bianchi, F., Kokkonen, T. V., Liu, Y., Kujansuu, J., Kerminen, V.-M., Petäjä T., Wang, L., Jiang, J. and Kulmala, M.: Variation of size-segregated particle number concentrations in wintertime Beijing, *Atmospheric Chemistry and Physics*, 20(2), 1201–1216, doi:10.5194/acp-20-1201-2020, 2020.

430

431

432

Figure caption

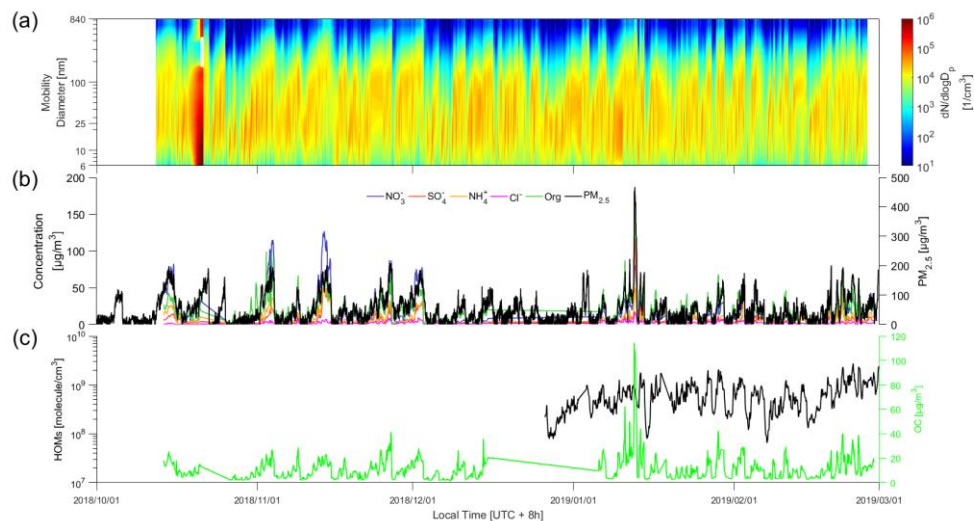


Figure 1. Time series of (a) particle number concentration distribution (PNSD) from 6 nm to 840 nm (b) chemical composition of NR\_PM<sub>2.5</sub> and PM<sub>2.5</sub> mass concentrations (c) The concentrations of organic carbon (OC) and highly oxygenated organic molecules (HOM).

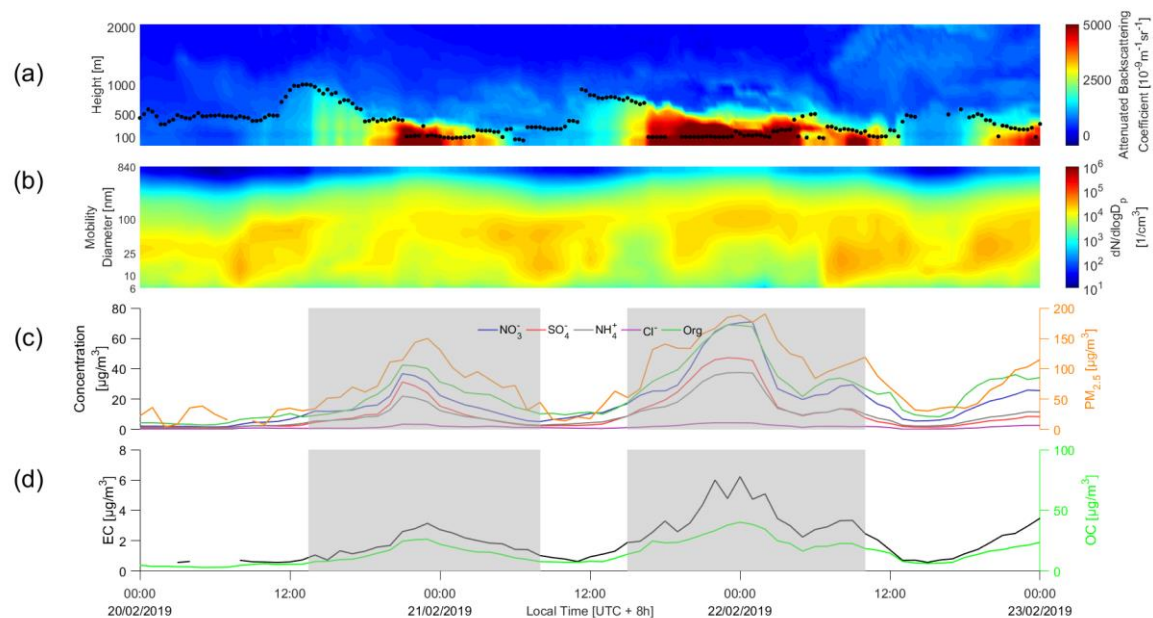


Figure 2. Time series of (a) attenuated backscattering coefficient and mixing layer height (b) particle number concentration distribution (PNSD), (c) chemical composition and PM<sub>2.5</sub> mass concentrations and (d) elemental carbon (EC) and organic carbon (OC). The haze periods are marked by the shaded areas.

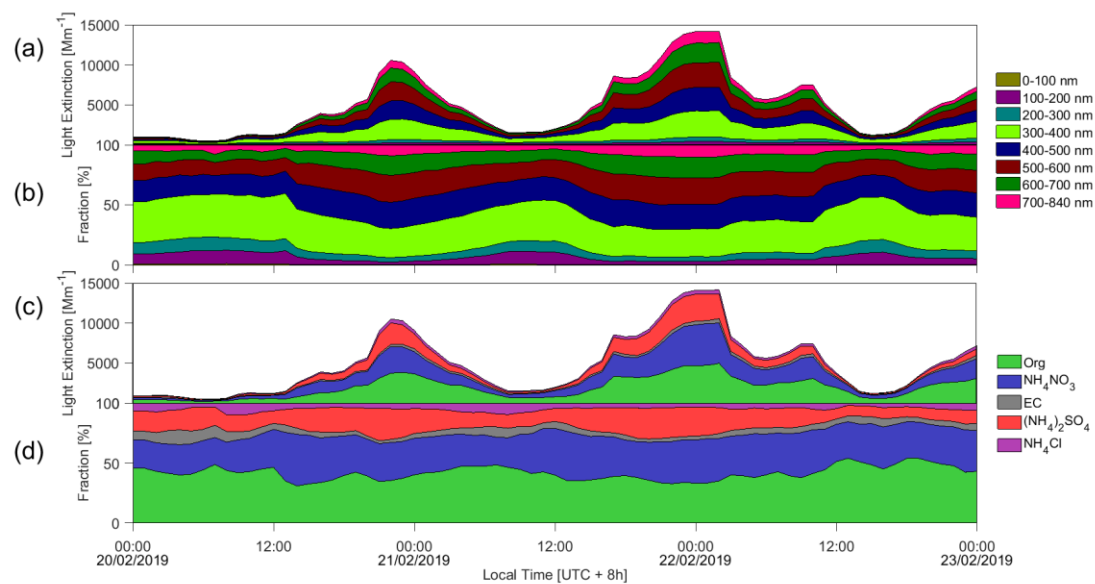


Figure 3. Time series of (a, b) variation of light extinction from different size aerosol and fractions, and (c, d) variation of light extinction from different aerosol species and fractions. The legends in the left side of figures are particle diameter and the right side are chemical compositions, respectively.

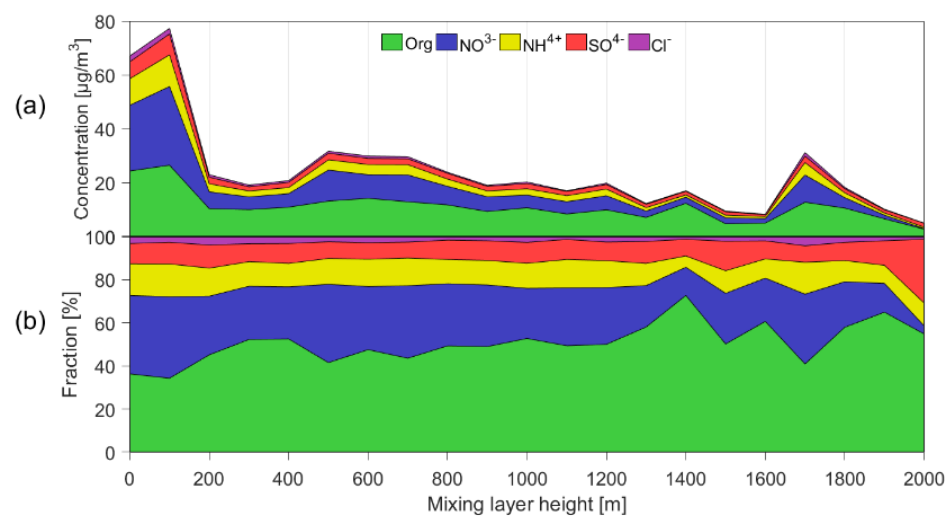


Figure 4. Statistical relationship between MLH and concentration (a) and fraction (b) of chemical composition species. Only daytime conditions determined by ceilometer from non-rainy periods (RH<95%) during the observation (~ 6 months) are considered.

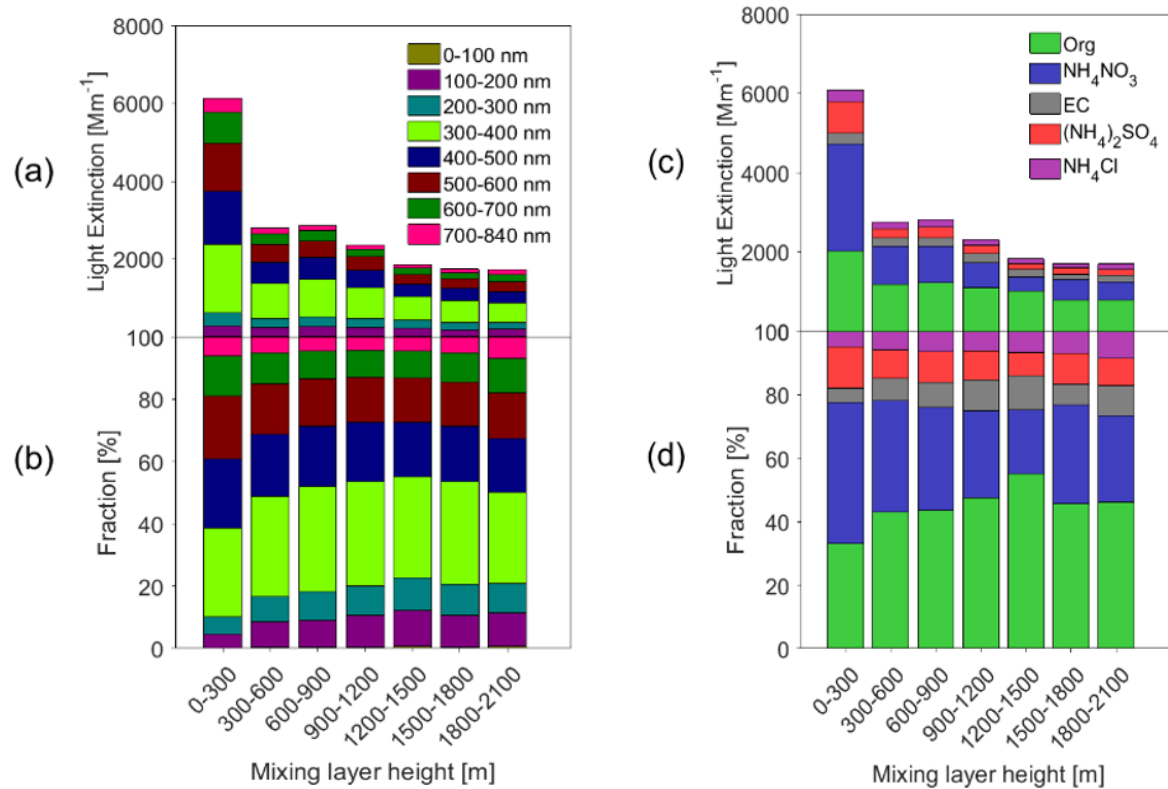
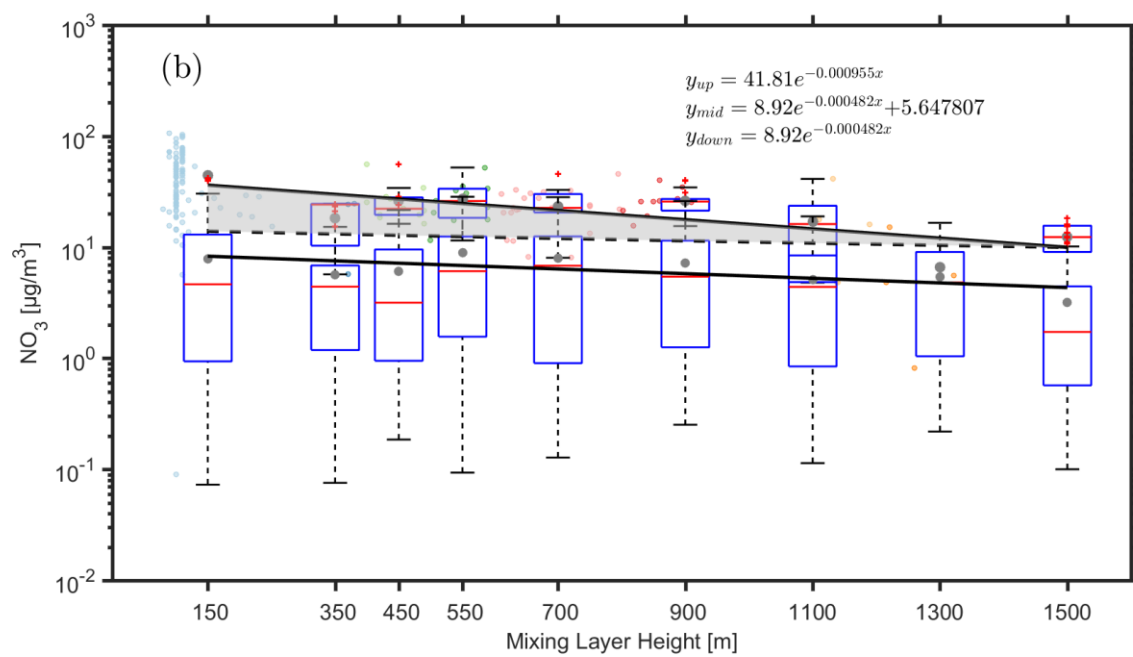
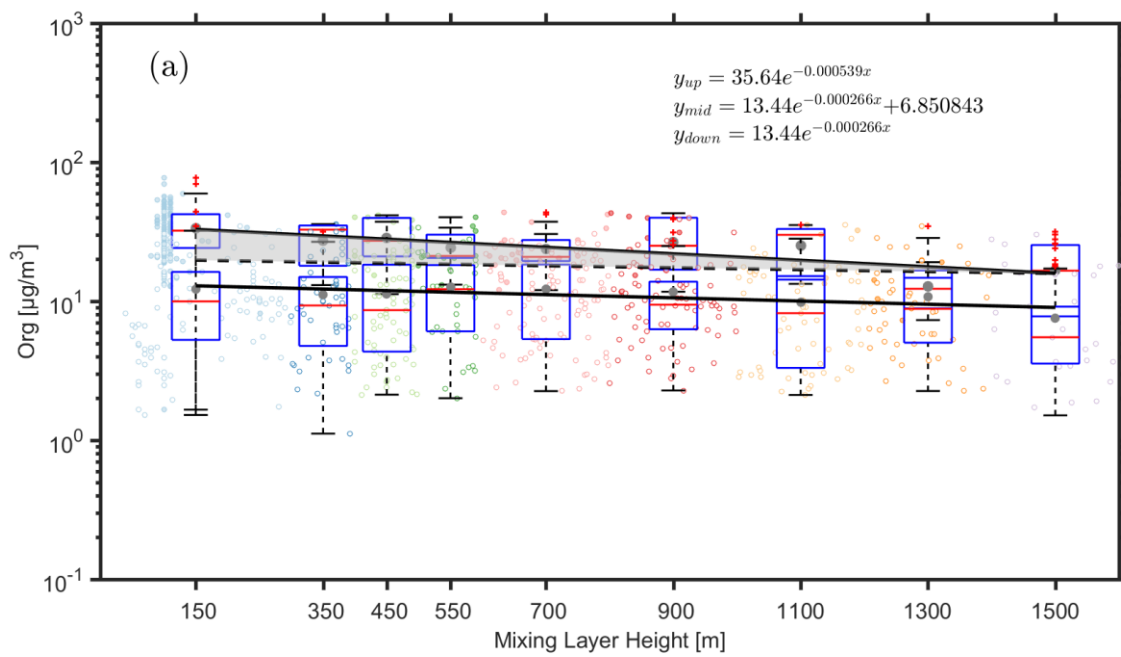


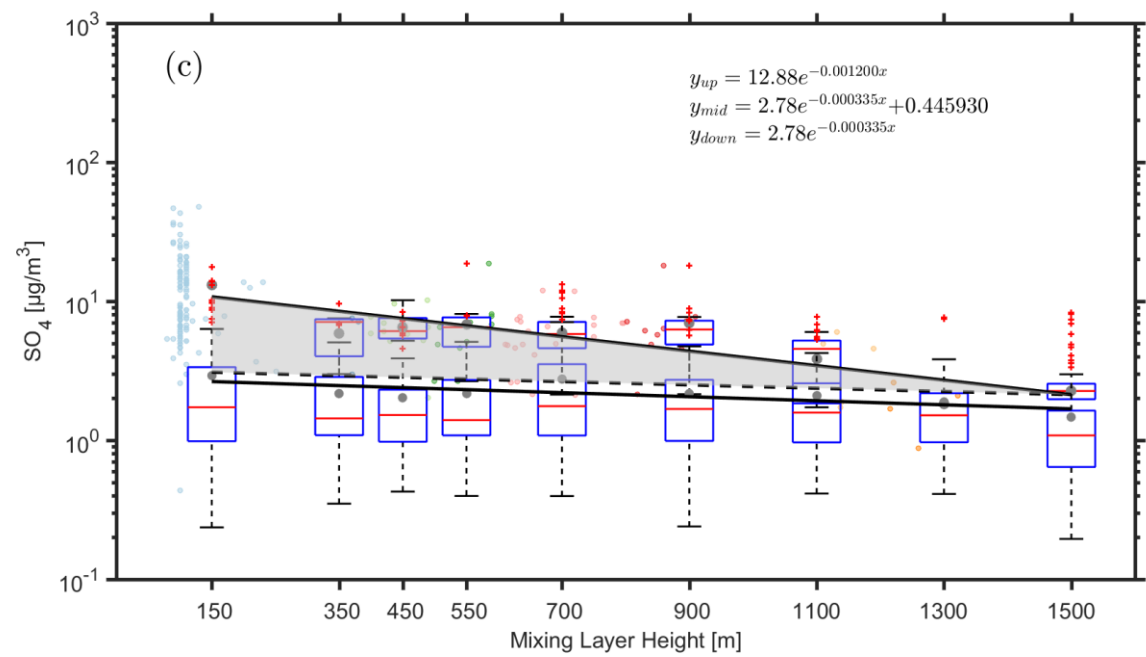
Figure 5. Statistical relationship between MLH and light extinction of different aerosol species.

Only daytime conditions determined by the ceilometer from non-rainy periods ( $\text{RH} < 95\%$ ) are considered.

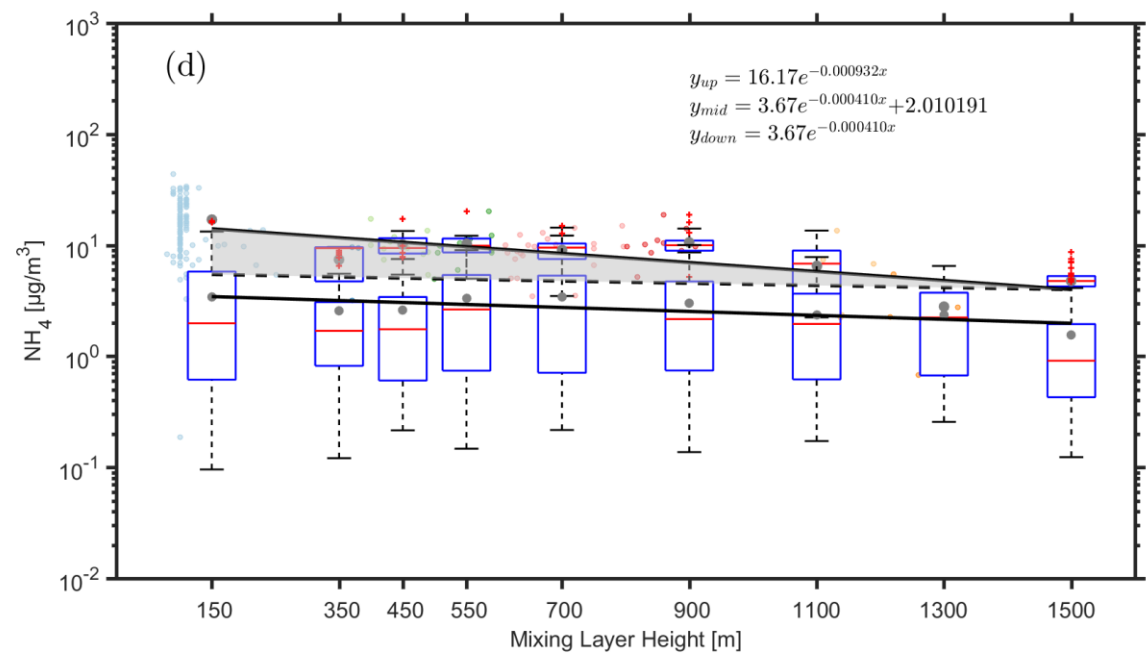


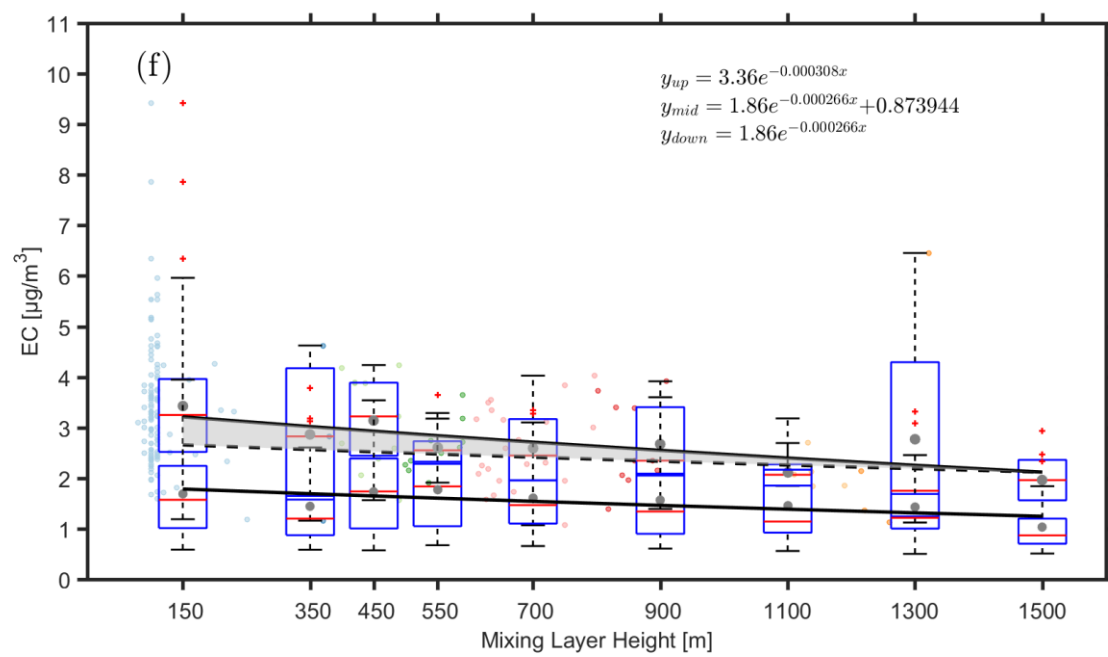
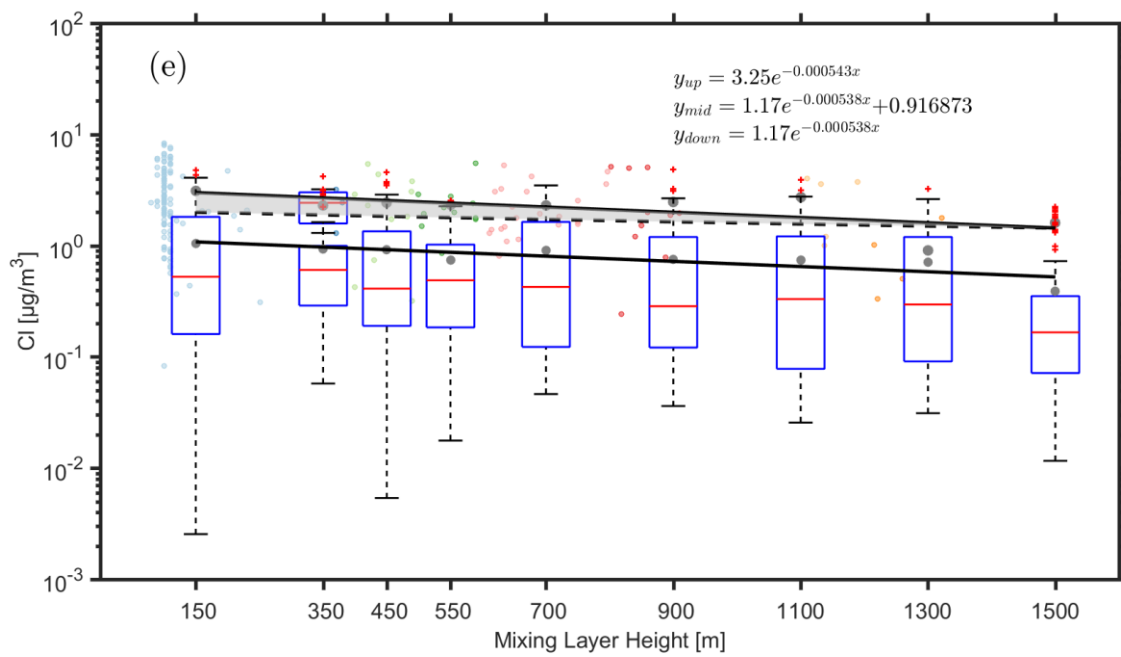


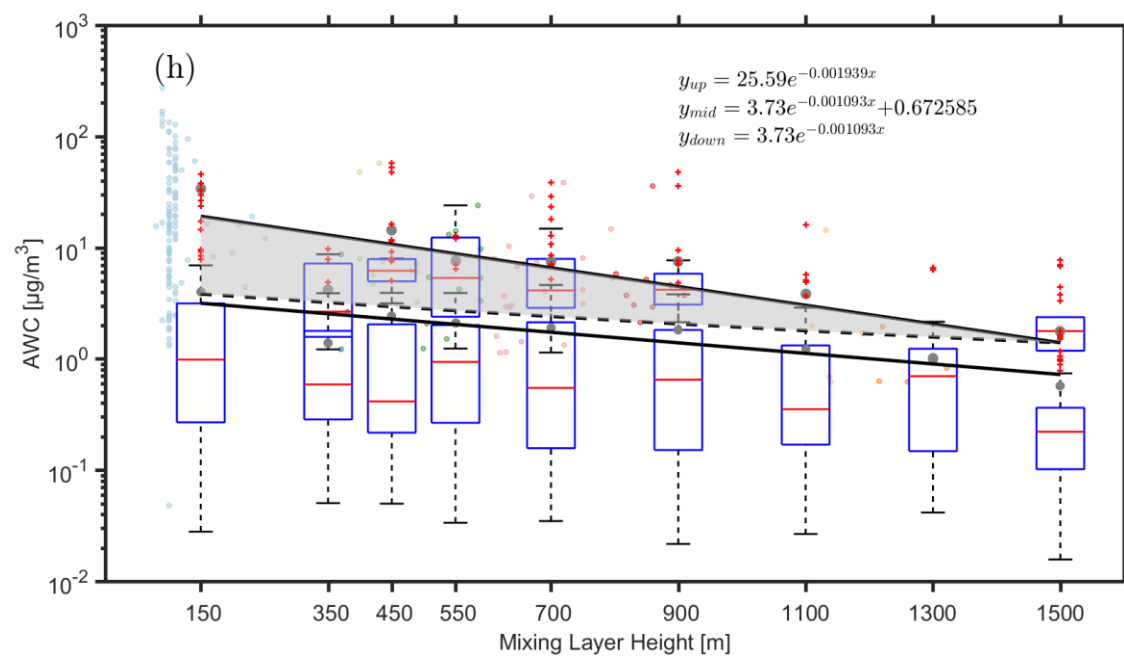
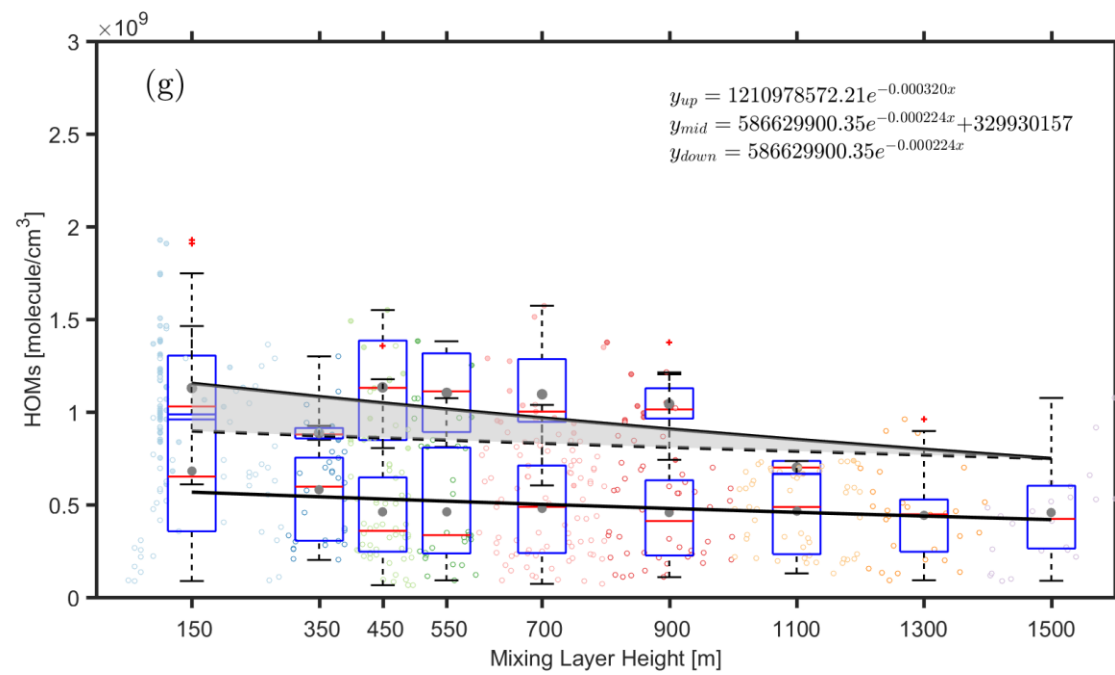
532



533







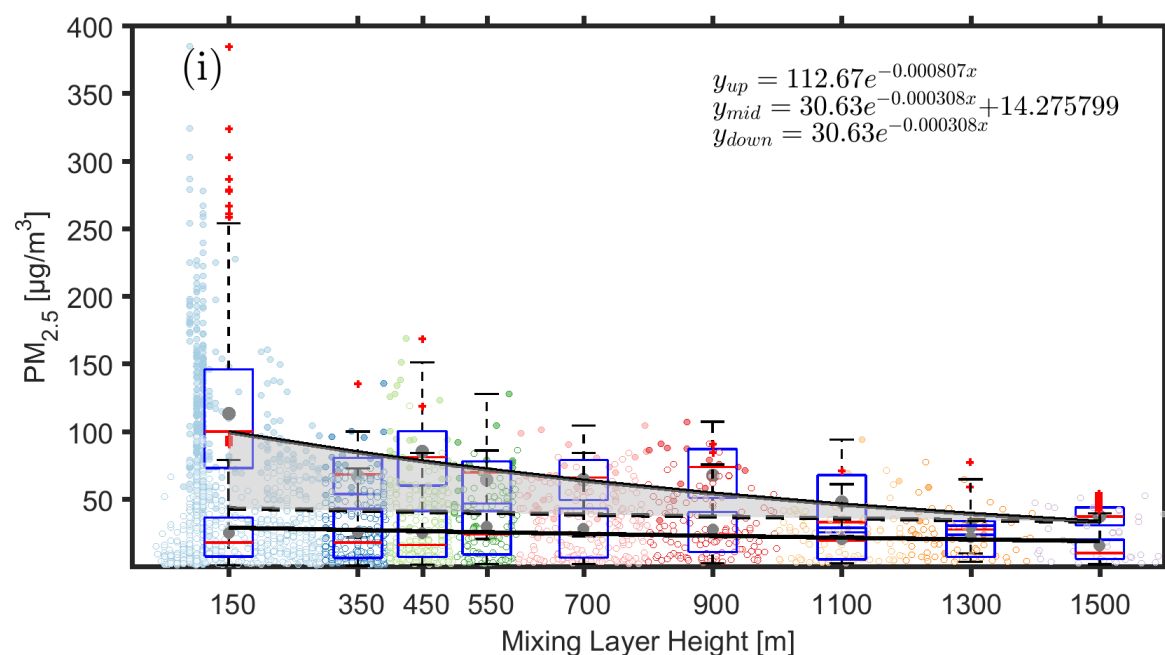
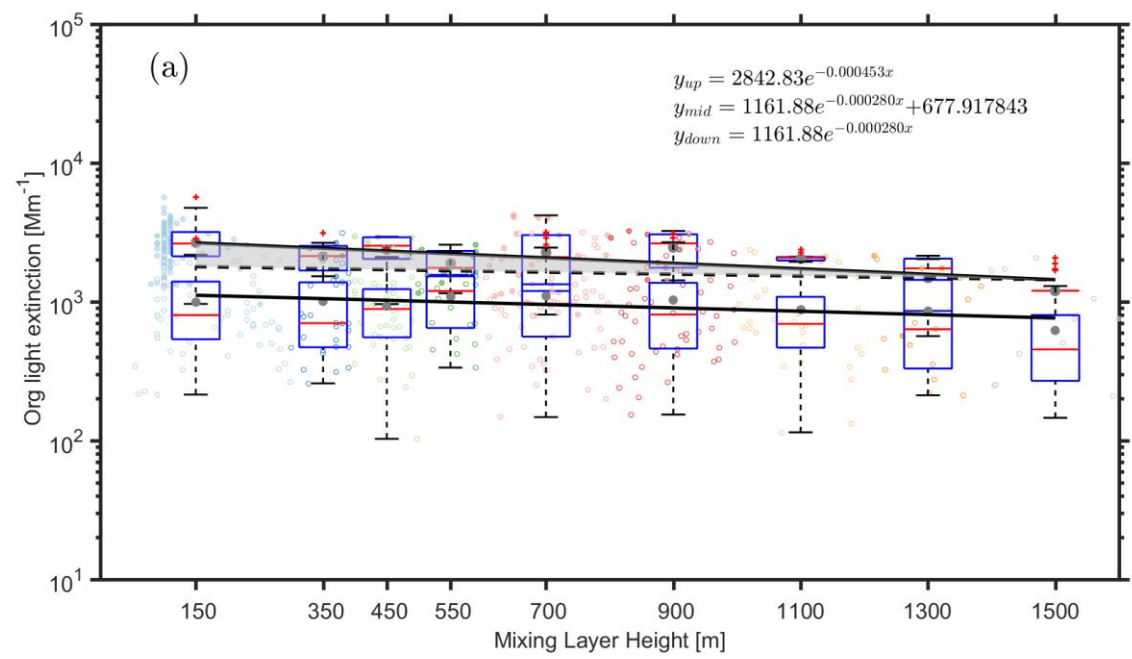
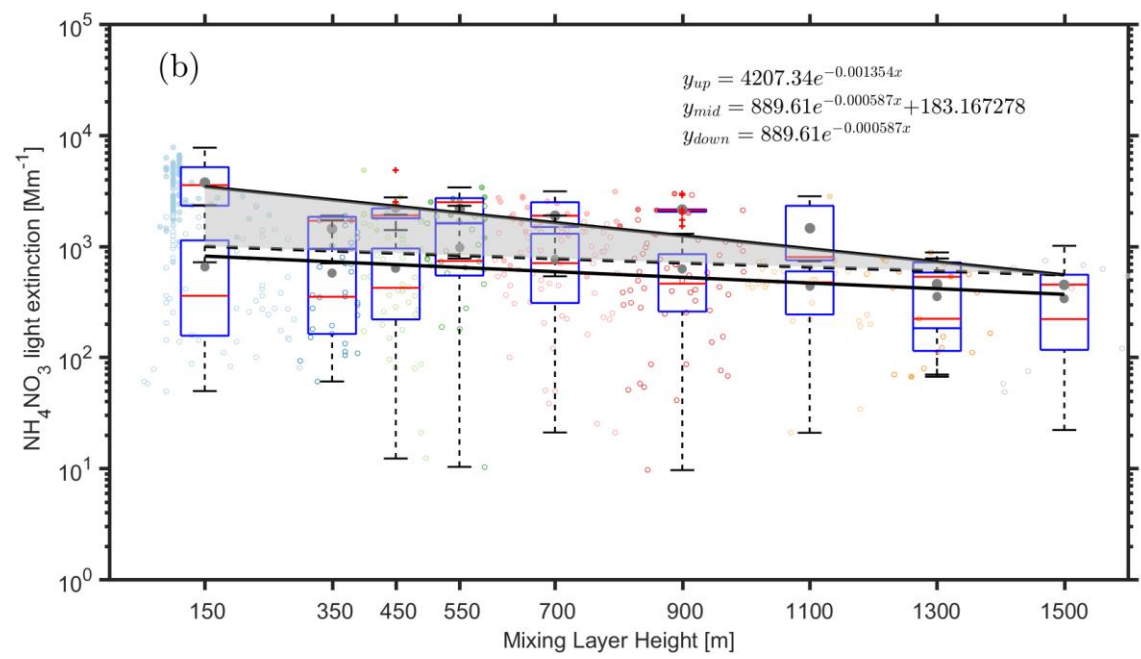


Figure 6. Observed dependency of (organics (a), nitrate (b), ammonium (c), sulfate (d), chlorine (e), element carbon (f), HOMs (g), AWC (h) and PM<sub>2.5</sub>(i) on the MLH during polluted and less-polluted conditions. The data related to the upper fitting line represents PM<sub>2.5</sub> concentrations larger than 75 µg m<sup>-3</sup>, while the data related to the lower fitting line represents PM<sub>2.5</sub> concentrations lower than 75 µg m<sup>-3</sup>. Only daytime conditions determined by the ceilometer from non-rainy periods (RH<95%) were considered. The solid circles and hollow circles denotes concentrations that are more than 75 µg m<sup>-3</sup> and less than 75 µg m<sup>-3</sup>, respectively. The dark grey points and red lines in the boxes represent mean and median values, respectively. The shaded area between the upper solid and dotted lines corresponds to an increased amount of the specific compounds with decreased MLH, assuming that the compound has the same variation pattern under highly- polluted conditions as in less polluted time.

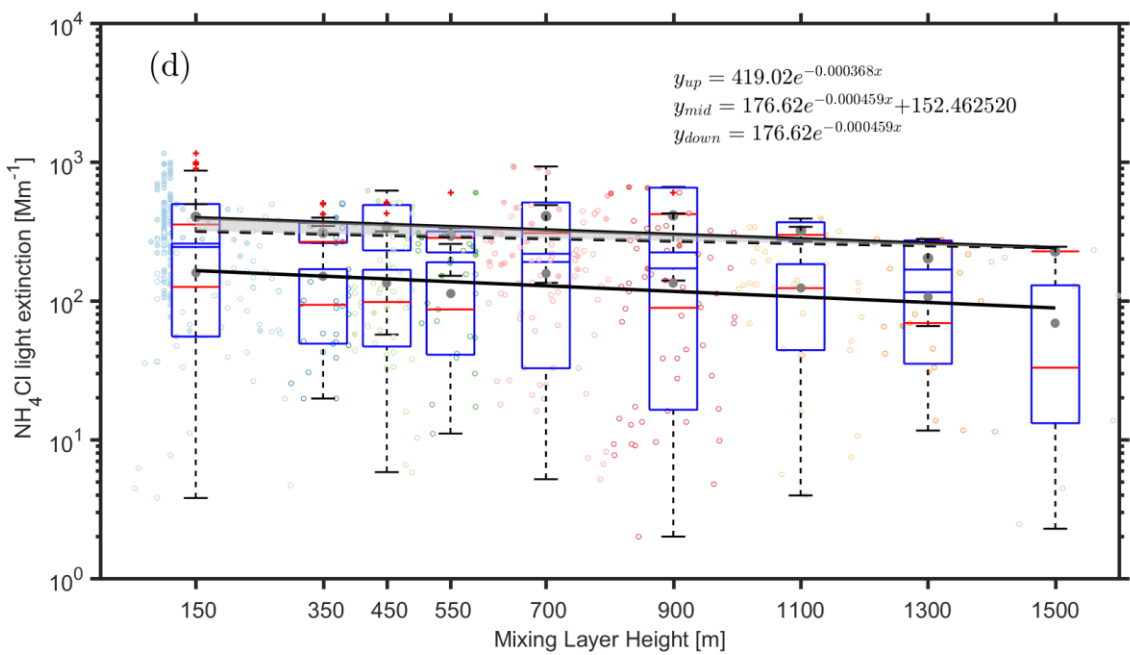
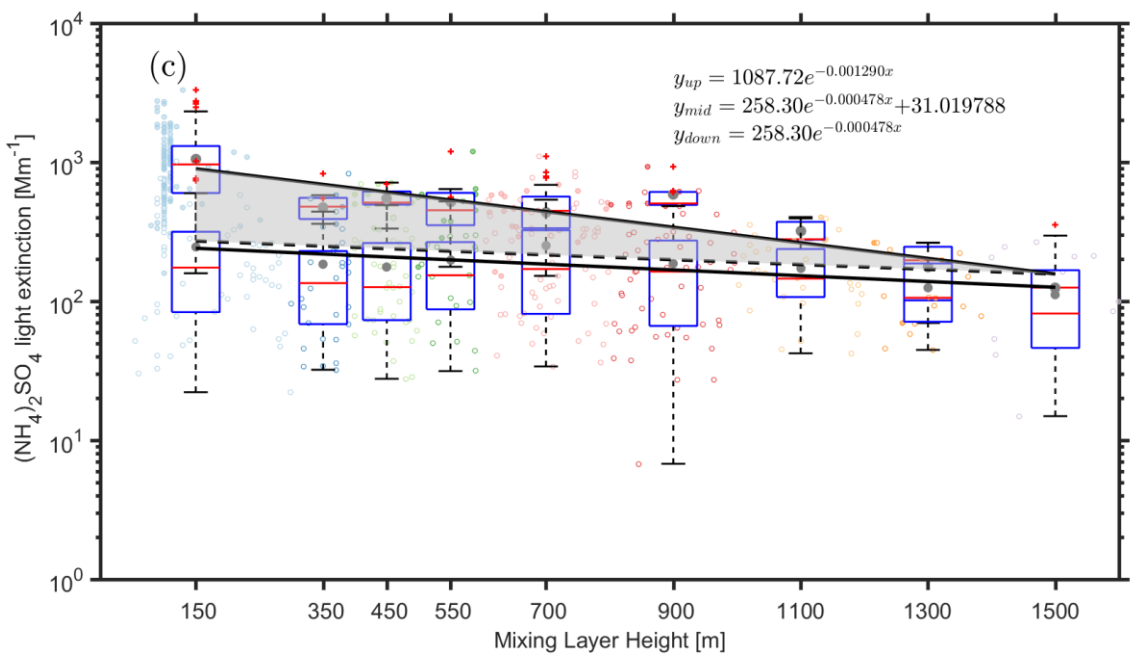
559  
560  
561



562



563



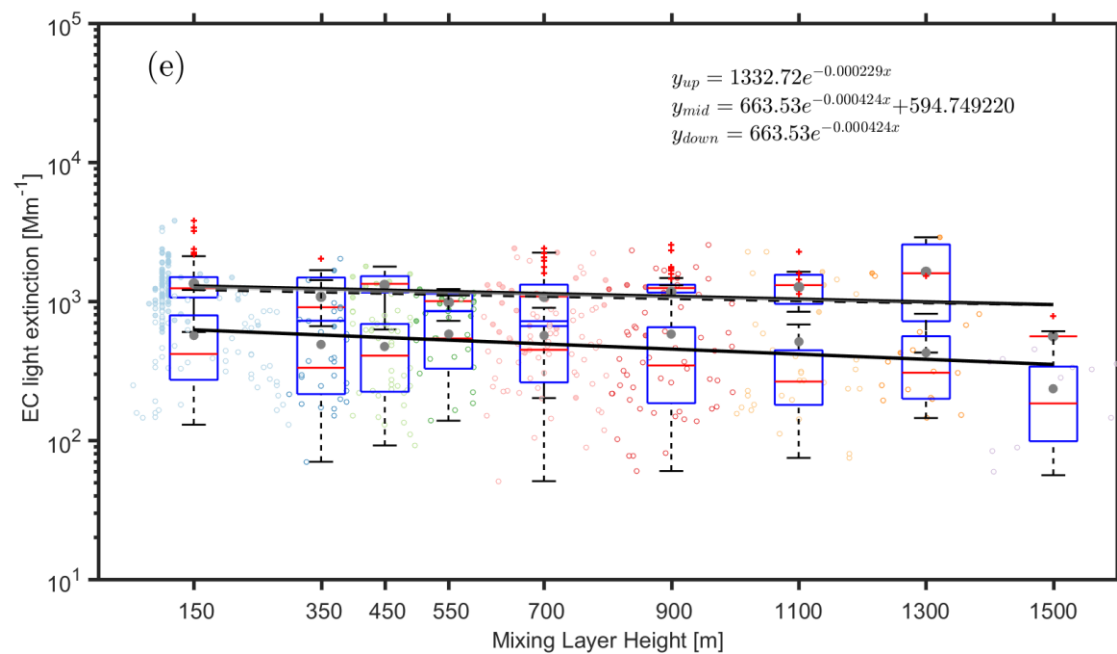


Figure 7. Observed dependency of the aerosol light extinction due to  $\text{NH}_4\text{NO}_3$  (a)  $(\text{NH}_4)_2\text{SO}_4$  (b),  $\text{NH}_4\text{Cl}$  (c) Org (d) and EC (e) on the MLH during polluted and non-polluted conditions. The data related to the upper fitting line represents  $\text{PM}_{2.5}$  concentrations larger than  $75 \mu\text{g m}^{-3}$ , while the data related to the lower fitting line represents  $\text{PM}_{2.5}$  concentrations less than  $75 \mu\text{g m}^{-3}$ . Only daytime conditions determined by ceilometer from non-rainy periods ( $\text{RH} < 95\%$ ) are considered. The dark grey points and red lines in the boxes represent mean and median values, respectively. The shaded area between the upper solid and dashed line corresponds to an increased amount of  $\text{PM}_{2.5}$  with a decreased MLH, assuming that  $\text{PM}_{2.5}$  has the same variation pattern under highly- polluted conditions as in less polluted time

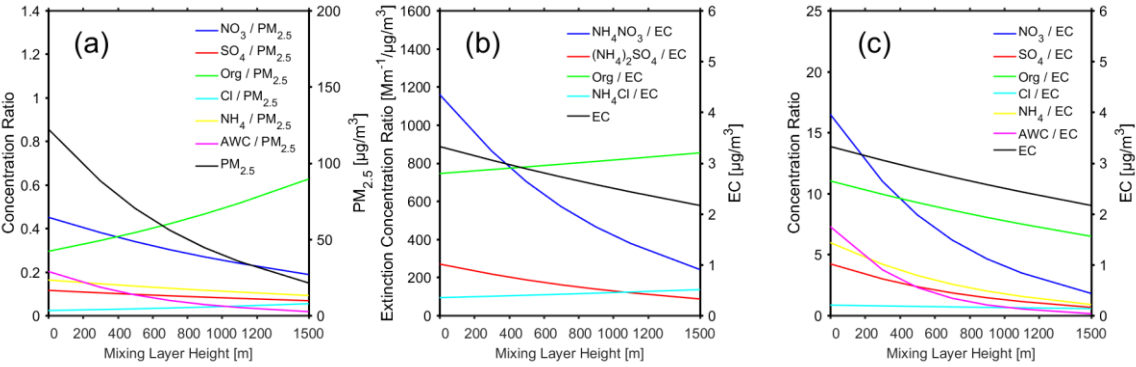


Figure 8. (a) the ratio of the mass concentration of different chemical components (nitrate, sulfate, organics, chlorine, ammonium) and AWC to the mass concentration of NR\_PM<sub>2.5</sub> as a function of MLH. (b) the ratio of dry aerosol light extinction by different chemical components (NH<sub>4</sub>NO<sub>3</sub>, (NH<sub>4</sub>)<sub>2</sub>SO<sub>4</sub>, Org, NH<sub>4</sub>Cl) to the mass concentration EC as a function of MLH (c) the ratio of the mass concentration of different chemical components (nitrate, sulfate, organics, chlorine, ammonium) and AWC to the mass concentration of EC as a function of MLH. All the data corresponds to polluted conditions (fine PM >75 μg m<sup>-3</sup>), and only daytime conditions determined by the ceilometer from non-rainy periods (RH<95%) were considered.



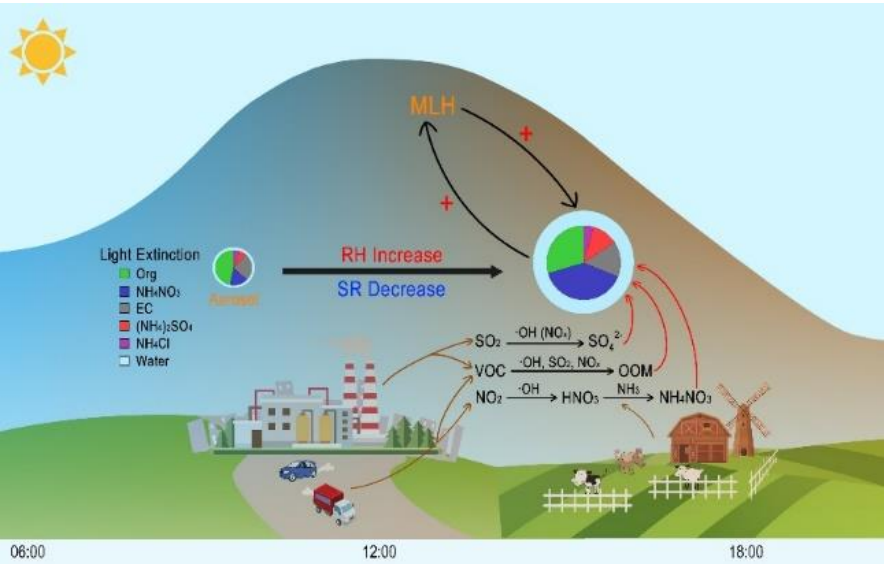


Figure 9. A schematic picture illustrating the process of rapid aerosol mass growth and enhanced light extinction in Beijing. The plus symbols represent the strengthening of a specific process. At the presence of aerosols during afternoon time in Beijing, the intensity of solar radiation reaching the surface will be decreased and relative humidity will be increased. As a result, the development of boundary layer will be suppressed, and the concentrations of aerosol precursors (e.g.,  $\text{SO}_2$ ,  $\text{NO}_2$ ,  $\text{VOC}$ ) will be increased. In turn, the secondary production of these sulfate, nitrate and oxygenated organic compounds will be enhanced due to increased concentrations and partitioning of these compounds into the aerosol phase. The increased formation of secondary aerosol mass will reduce solar radiation further and the haze formation increased, as shown in pie charts that the light extinction fraction of aerosol changed from organic to nitrate. Noting that during intensive haze periods, nitrate and its contribution to light extinction contribution increased dramatically.

